Ore Geology Reviews 154 (2023) 105279

Contents lists available at ScienceDirect

Ore Geology Reviews

journal homepage: www.elsevier.com/locate/oregeorev

Mineralogical constraints on the genesis of an alkalic-type epithermal Au-Te deposit: Tuvatu, Fiji

Rose Clarke [a], Daniel J Smith [a], Jonathan Naden [b], David Holwell [a], Stephen Mann [c]

[a] Centre for Sustainable Resource Extraction, University of Leicester, University Road, Leicester LE1 7RH, United Kingdom
[b] British Geological Survey, United Kingdom
[c] Lion One Metals, Nadi, Fiji

ARTICLE INFO

Keywords:
Tuvatu
Alkaline
Gold
Telluride
Low-sulfidation
Fiji

ABSTRACT

To study the characteristics and genetic constraints on alkalic-type epithermal Au mineralisation, here we use the example of the Tuvatu Au-Ag deposit in Fiji, with an emphasis on detailed, quantitative mineralogy. Tuvatu mineralisation is hosted in a weakly altered potassic monzonite in parallel sided-veins of K-feldspar, biotite, sericite, calcite, and quartz, with epidote-bearing propylitic or sericite-rich selvages. Petrographic study of core and automated SEM-based mineralogical mapping of thin sections have been utilised to update previous parageneses of the deposit. Automated SEM techniques enable identification of small amounts of obscure minerals that form minuscule grains, which would otherwise be very difficult to identify and measure. As a result, our data show that gold fineness is extremely high, with the mean and median Au content of native-Au and Au-Ag alloy being 96.7% and 100% respectively, yet precious-metal tellurides make up the majority of the Au deportment. Tellurides show evidence of multiple phases and zoning with depth. For the first time at Tuvatu, Pt- and Pd-tellurides have been identified. Tuvatu has a number of features in common with alkalic systems elsewhere, including quartz-poor, carbonate-rich veins and alteration, abundant and varied telluride minerals, high gold grades, and Pt-Pd occurrences. We suggest these characteristics are a result of relatively high temperature (250–300 °C) fluids and immiscible semi-metal melts fluxing into the shallow epithermal environment. High pH fluids lead to quartz-poor alteration, but mildly acidic conditions dominate in areas of high fluid flux, where the lower pH causes precipitation of tellurides with quartz. Boiling of the fluids produces zonation of tellurides with depth but leaves relatively subtle textural evidence compared to boiling in most epithermal systems, in common with other quartz poor, carbonate-rich alkalic epithermal deposits around the world.

1. Introduction

Epithermal- and porphyry-type deposits with a close spatial and temporal association to alkaline magmatism commonly contain exceptional Au grades, tonnages, or both (Jensen & Barton, 2000; Pals & Spry, 2003). In addition to precious metal endowments, alkalic deposits may be distinguished from more common sub-alkaline equivalents, typically calc-alkaline hosts (du Bray, 2017), on the basis of contents of critical elements such as Te, V, and Bi (Ciobanu et al., 2006; Cook et al., 2009; Jensen & Barton, 2000; Kelley & Spry, 2016; Richards, 2009). Alkalic deposits most commonly occur in tectonic environments where extension of subduction-associated volcanic arc terrains has occurred, sometimes referred to as "post-subduction" (Jensen & Barton, 2000; Richards, 2009).

It remains unclear whether the world's alkalic deposits, including Cripple Creek, Colorado; Porgera, Papua New Guinea; and Vatukoula, Fiji, represent a distinct subclass of epithermal deposits. The post-subduction setting perhaps allows for magma sources that ultimately feed hydrothermal systems with characteristic precious and semi-metals, as well as the signature alkaline composition: low-degree partial melts of metasomatised lithospheric mantle (Blanks et al., 2020; Ciobanu et al., 2006; Holwell et al., 2019), or melting of earlier arc magma cumulates (Clarke et al., 2022; Richards, 2009) for example, may be key in determining the fertility of post-subduction magmas The alkaline host rocks potentially influence the ore-forming hydrothermal fluids, by buffering to pH conditions not typically attained in sub-alkaline hosts, and thus facilitating transport of semi-metals such as tellurium in solution (Smith et al., 2017).

Tellurium-bearing minerals, including those formed with precious metals, are a defining feature of the alkalic subclass, and the evolving

E-mail address: rose@satarla.com (R. Clarke).

https://doi.org/10.1016/j.oregeorev.2022.105279
Received 12 June 2022; Received in revised form 27 September 2022; Accepted 29 December 2022
Available online 2 January 2023

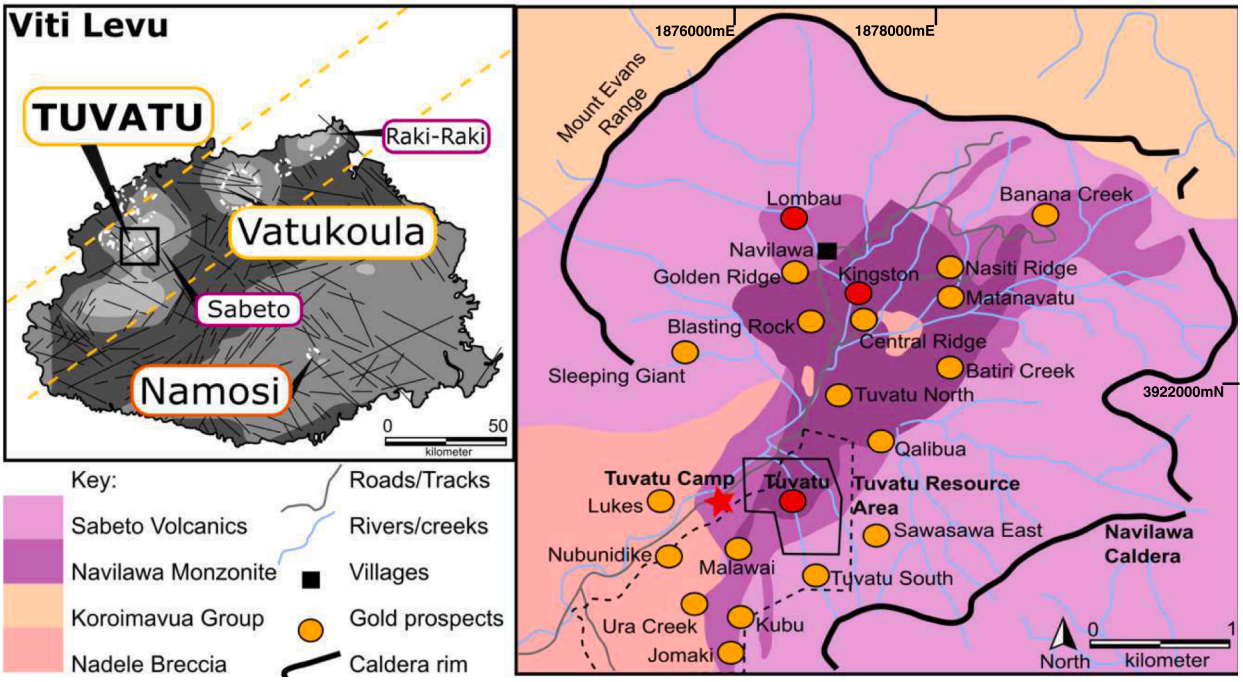

Fig. 1. Left: Map of Viti Levu, the mineralised gold belt, and noteworthy deposits. White dashed lines show caldera rims. Gravity contours in mgal: dark grey = 0, mid grey = 1–20 and light grey = 20 +. Black box shows area of map right. Right: Base map of the Navilawa Caldera, with main lithological groups and geographical features annotated. The centre of the caldera is composed of the intrusive Navilawa monzonite, the intrusive equivalent of the Sabeto volcanics which make up the rest of the caldera. Their unconformable relationship with surrounding subduction material can be seen. Other prospects within the caldera are also noted as gold dots, and the dashed black line outlines the Tuvatu resource area.

Table 1
Lode 'sets' or groups, with the individual lodes that comprise them, typical strike, and dip they show.

Lode set	Description	Strike	Average Dip
H	H1, H2	NW-SE	80 SW
Tuvatu (T)	Tuvatu 1 (T1), Tuvatu 2 (T2)	NW-SE	75 SW
Murau	Murau 1, Murau 2, Murau 3, and associated hanging wall, foot wall, and flatmate lodes	E-W	~80 S
Nasivi	Nasivi	NE-SW	35 E
Snake	S1, S2, and associated hanging wall and foot wall lodes	E-W	70 S
SKL	SKL1, SKL2, SKL3, SKL4, SKL5, SKL6, SKL7, SKL8, SKL9; all 'stockwork' veins	~NE-SW	~40
GRF	GRF 1; GRF 2; GRF 3	N—S	
Upper Ridges	UR1, UR2, UR3, UR4, UR5, UR6, UR7, UR8, and associated foot wall, hanging wall, and extension lodes	N—S (some swinging)	~75 (S)E
Upper Ridges West	URW1, URW2, URW3, and associated footwall and hanging wall lodes	N—S	80
West	West 1, West 2, West 3, West 4, West 5, West 6, West 7,, and associated footwall and hanging wall lodes	E-W	70 N

genetic models commonly incorporate tellurium geochemistry to illustrate processes. Detailed, quantitative mineralogy is vital for building the complex paragenetic sequences of alkalic deposits and determining the role of melt source and fluids in ore formation, not least due to the obscure minerals found, and the often small grain size of precious and semi-metal baring minerals. Here we provide a deposit-scale study of the Tuvatu deposit, the second largest known Au-Ag-telluride deposit in Fiji (Scherbarth & Spry, 2006). We present detailed geochemical, textural, and quantitative mineralogical data to gain a better understanding of Tuvatu and consider its place within models for alkalic-type epithermal deposits in general.

2. Regional geology and mineralisation

Fiji is located on the complex boundary between the Pacific and Indo-Australian Plates, now a broad zone of island arcs, ridges, transform faults, and back-arc basins. Prior to the Late Miocene, subduction ensued as the Pacific Plate subducted beneath the Indo-Australian Plate along the Vitiaz Trench. Collision of the Melanesian Border Plateau and Ontong-Java Plateau halted subduction (Begg & Gray, 2002; Hathway, 1993), choking the trench and triggering arc-polarity reversal and fragmentation, formation of a left-lateral transverse rift, and rotation of Fiji (Gill & Whelan, 1989; Taylor et al., 2000). Alkaline magmas and associated Au-Ag-Cu prospects formed during this reorganisation, and are found throughout Papua New Guinea, the Solomon Islands, and Fiji (Holm et al., 2019).

Volcanic rocks in Fiji record proto- to mature-arc activity in the Yavuna Group and the Wainimala Group respectively (Hathway, 1993; Wharton et al., 1995). Extension ended direct subduction of the Pacific Plate beneath Fiji (Colley & Hindle, 1984). At approximately 5 Ma, "post-subduction" shoshonitic lavas were erupted (Gill & Whelan, 1989), although geochemical characteristics remained subduction-like (Rogers & Setterfield, 1994). The ~5 Ma shoshonitic rocks are associated with approximately contemporaneous mineralisation across Fiji (Forsythe et al., 2019), and distribution (Fig. 1) suggests a strong structural control (Hathway, 1993).

2.1. Deposit geology

Tuvatu is currently operated by Lion One Metals. The deposit resides in the SW corner of the Navilawa Caldera, part of the mineralised gold belt that crosses the west of Viti Levu (Fig. 1). Both the Gold Belt and Navilawa Caldera contain multiple prospects. Within the caldera, the subduction-associated Nadele Breccia, a sequence of volcaniclastics, basalts, and minor limestones, are intruded by monzonites. The

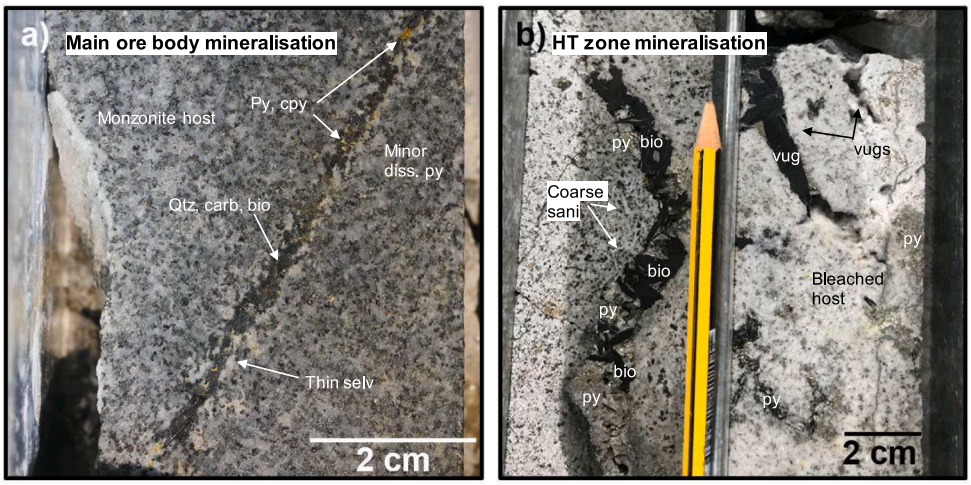

Fig. 2. Photographs of drill core showing the two main styles of mineralisation observed at Tuvatu. a) drill core containing an isolated thin quartz (qtz) and sulfide stringer with visible pyrite (py) and chalcopyrite (cpy), with a thin selvage and no visible extensive alteration into the host rocks; b) bleached drill core, with the left-hand side showing a coarser biotite (bio)-quartz-sulfide vein in rock altered to contain abundant coarse sanidine (sani) crystals, and the right-hand side showing extensive sulfide mineralisation into altered host rock dominated by quartz and feldspar.

monzonites are thought to be the intrusive equivalent of post-subduction shoshonitic lavas, are dated at 4.85 Ma, and all are potassic (Clarke et al., 2022). Samples from Tuvatu are dominantly composed of feldspar (which makes up >50% of sample area); they also contain abundant clinopyroxene and biotite phenocrysts. Propylitic through to weak sericitic alteration is pervasive. Alteration minerals include abundant epidote; minor quartz; magnetite; euhedral apatite; disseminated pyrite; and brown clays. Younger, undated andesitic dykes crosscut other lithologies (Scherbarth & Spry, 2006), and there is evidence that some are weakly mineralised. Two structures cross the deposit with an east–west strike: the CABX Fault (a calcite-cemented breccia with vugs and cavities filled with calcite) and the Core Shed Fault (a region of disintegrated monzonite with calcite alteration). No veins are clearly offset or cut by the faults. The Core Shed Fault is not mineralised, but traces (<2 g/t) of Au have been measured in the CABX Fault.

The ores are hosted in 'lodes', 47 of which are noted in the 2020 PEA prepared for Lion One. These lodes comprise zones of narrow veins, individually ranging from 1 to 200 mm wide. Widths of > 10 m have been measured but, in many cases, are thought to be intersections of multiple lodes. As outlined in Table 1, individual lodes have been grouped based on spatial data. Rather than a stockwork-type morphology, each lode group is made up of parallel veins, or anastomosing networks of veinlets which are contained in boundaries generally parallel to the overall dip and strike of the lode. Whilst groups show differing orientations and dips, they are morphologically and mineralogically similar. Most lodes are composed of calcite-feldspar-quartz-pyrite ± biotite and sulfides, and contain Au present as native-Au, Au-Ag alloy, and/or tellurides. The other style of lodes occurs in the 'HT Zone', which is made up of the four combined H and Tuvatu (T) lodes, reported by the company and in prior literature (Scherbarth & Spry, 2006; Spry & Scherbarth, 2006) as being visibly, geochemically, and mineralogically distinct. Thicker quartz-pyrite-magnetite veins, coarse biotites (up to 3 cm), and more abundant sulfide phases characterise these rocks. The differences between the lode types are evident in drill core and outcrop (see core photographs in Fig. 2).

3. Sampling, materials, and analytical methods

3.1. Sampling methods

A total of 275 samples were collected from Tuvatu; 263 samples of drill core, and 12 of which are outcrop or rock samples obtained from the decline. Samples were collected in 2017 and 2019. Metadata from samples, including their depth and location can be found in Appendix A.

3.2. Analytical methods

3.2.1. Geochemical data

The geochemical data used in this study are primarily from the Lion One database, which includes assay data compiled from various companies since the discovery of the deposit. Data prior to 2019 were mainly obtained from half drill core samples sent to ALS in Townsville, Australia, where samples were crushed, pulverised, and analysed via fire assay with an AAS finish. Samples with Au grades above 3 g/t were re-assayed. Lion One now has a laboratory facility at its office in Nadi, Fiji, where the same procedure is followed. Assay results are sent to database consultant rOREdata Pty ltd in Perth, where they are validated, merged with geological logging data, and checked for consistency, quality assurance (QA)/quality control (QC), and duplicates.

3.2.2. Sample preparation and SEM analysis

Thin sections of samples with visible mineralisation were cut to include as much vein and alteration as possible. Optical microscopy was conducted on all thin sections. Data was collected from 15 thin sections using a Zeiss SIGMA 300VP scanning electron microscope, equipped with two Bruker XFlash 6|60 energy dispersive (ED) spectroscopy detectors, with 126-eV energy resolution. Operating conditions included an accelerating voltage at 20.01 kV, an aperture size of 120 μm, and a working distance of 8.5 mm. Data were collected and processed using Zeiss Mineralogic, software that provides automated mineralogy based on quantitative ED spectra. This is done using a mineral list composed by the user (part of Appendix B), and within other constraints set, such as magnification, pixel size, and dwell time. As minerals are identified based on chemistry, minerals with light elements (such as C or H that are not accurately identified using automated SEM), or minerals with similar bulk compositions (e.g. magnetite vs hematite), may be misidentified (Schulz et al., 2020). Conversely, solid solutions may be overspecified. User-defined limiting factors such as upper limits (which may be as low as 0.01%) for a certain elements can help distinguish similar mineral chemistries and solid solution series. The software allows image processing and reports analysis of grains, including associations, inclusions, average size, and average mineral compositions.

Each section was first run at a coarser scale (30x30 μm pixel size) to provide full mineralogical mapping. This is referred to as the 'modal run' in this study. The second utilised a bright phase search, performed at a much finer scale (~250x magnification, with a 700 nm^2 pixel size), at low brightness and high contrast so that only phases with high electron backscattering (approximating to a high bulk atomic number) were visible. Phases were mapped where specific requirements were met, i.e., phases bright enough to be visible, and within size constraints set (<200

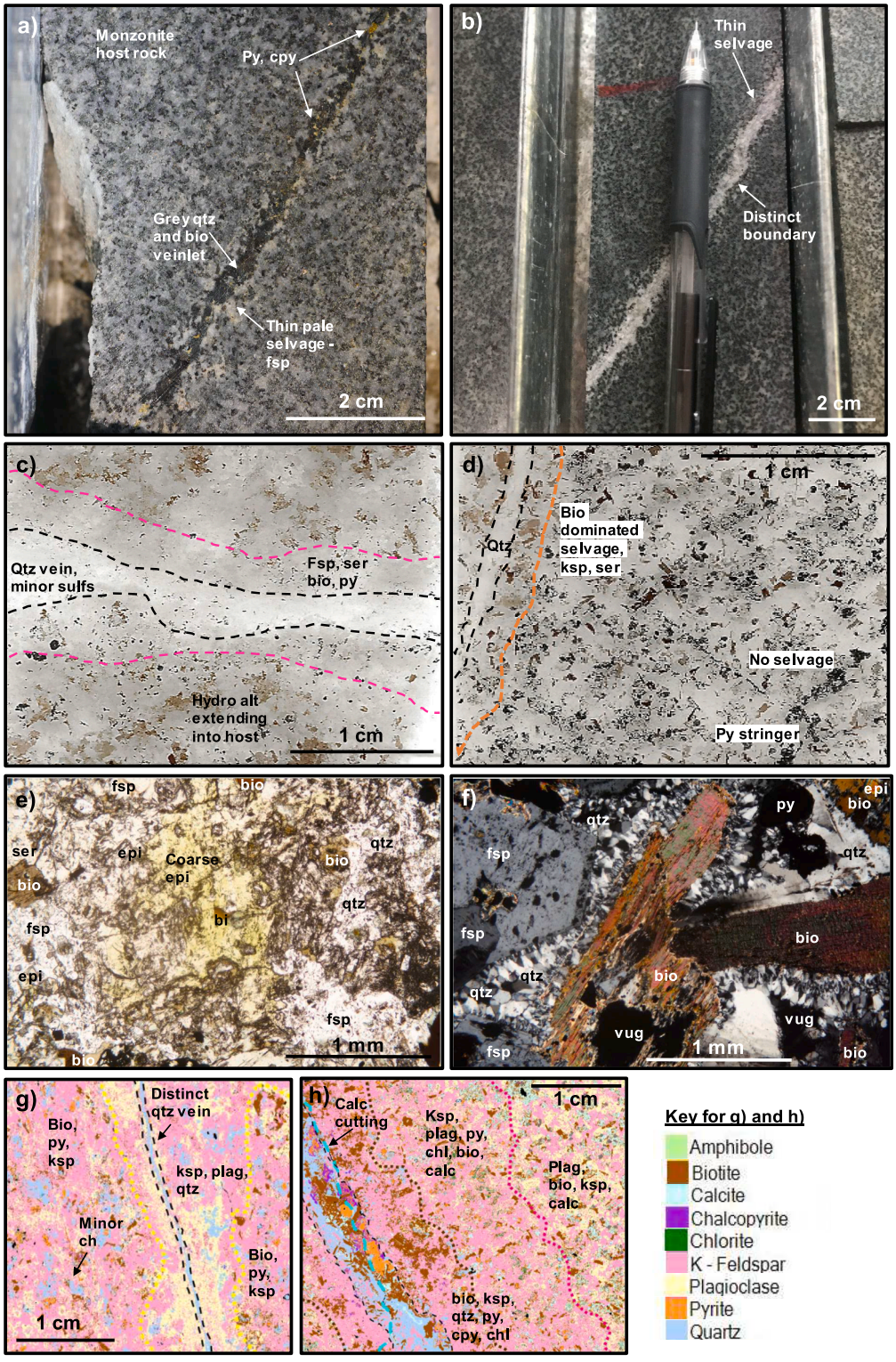

Fig. 3. A) photograph of drill core, showing a thin sulfide stringer within a zoned selvage; adjacent to the sulfide stringer, biotite is the dominant phase, passing into sericite and then to monzonite host rock; b) photograph of drill core showing a stringer within a bleached selvage, in part of core where monzonite has been altered by hydrothermal biotite overprinting; c) scan of a thin section, showing a quartz vein within a pale selvage dominated by quartz, sericite and fine disseminated pyrites and minor biotite; d) thin section scan showing a quartz and calcite vein within a biotite dominated selvage; e) photomicrograph showing a coarse apple-green epidote crystal associated with smaller epidote crystals, minor hydrothermal biotite, and quartz; f) photomicrograph in cross-polarised light showing coarse hydrothermal biotite alongside vug-filling quartz, anhedral pyrite and coarse feldspars; g) thin section modal scan colourised with zeiss mineralogic automated mineralogy, showing a quartz stringer within a bleached selvage dominated by plagioclase and quartz; and h) thin section modal scan coloured with zeiss mineralogic automated mineralogy, showing a quartz vein cut by calcite stringer, and another zoned selvage (whereby the first zone is composed of biotite, then the second potassium feldspar and chlorite). (For interpretation of the references to colour in this figure legend, the reader is referred to the web version of this article.)

μm^2) to avoid time consuming mapping of coarse-grained minerals, particularly galena. Any coarser phases were large enough to be identified in the first run. Once identified, individual grains (n = 2126) were mapped, along with a 5 μm halo around them, and studied manually to note chemistry, grain area, grain shape, and the setting/minerals the grain is hosted in. This review also allowed mixed pixels to be resolved, in addition to equivocal analyses and overlaps. For full details and examples of mineral libraries, see Appendix B.

4. Results

4.1. Alteration assemblages

4.1.1. Main Zone

Veins within the Main Zone (i.e., the main ore body) are composed of quartz, carbonates, and sulfides, and have sharp, distinct margins. Whilst minor alteration is abundant throughout the deposit, strong alteration of the wall rock is restricted to selvages, within millimetres to

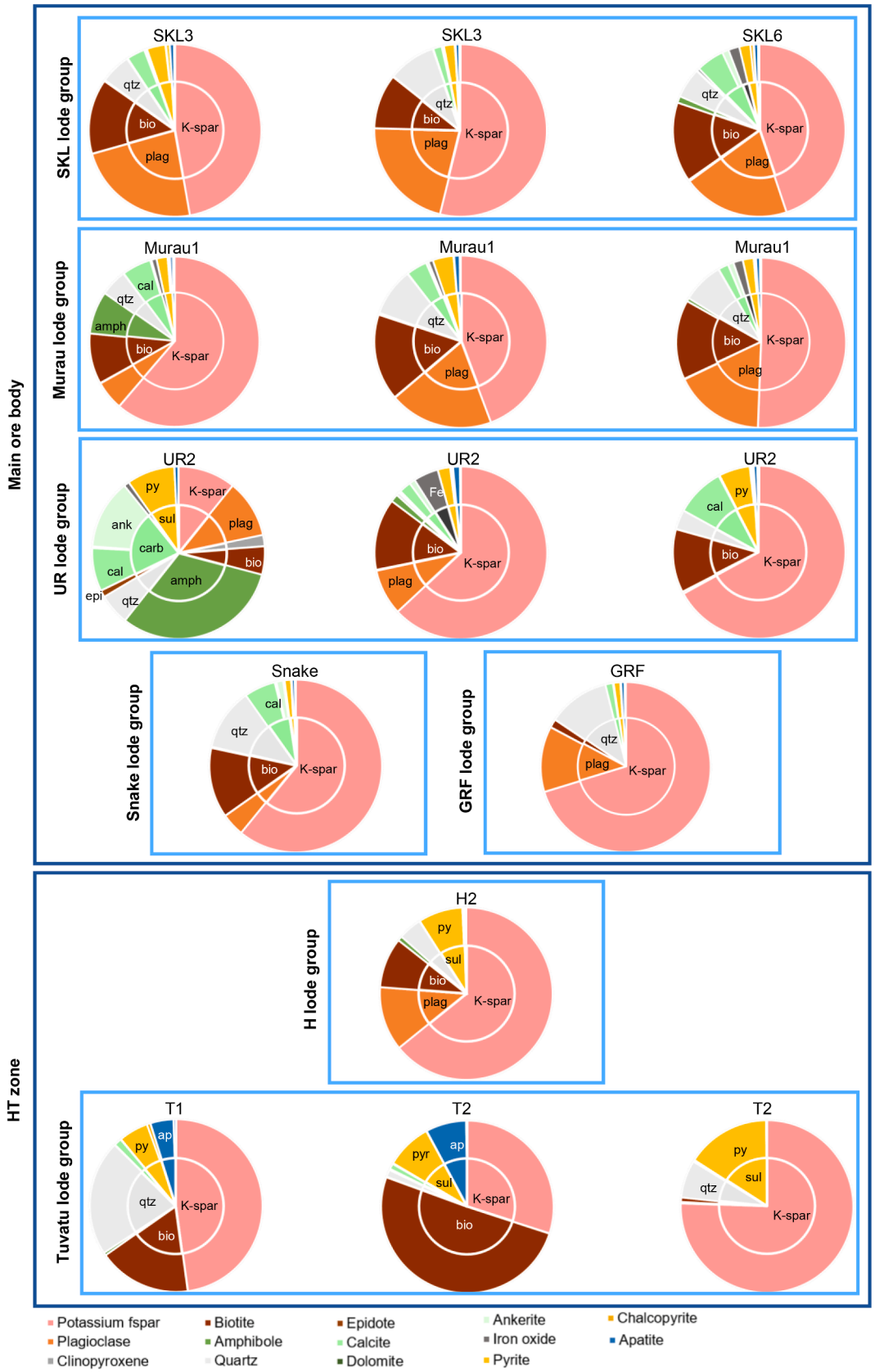

Fig. 4. Pie charts showing the bulk modal compositions of each thin section scanned on the Zeiss and classified and mapped using Mineralogic. Thin section name and lode hosted within the thin section is above each pie. Within each pie chart there is a smaller, inner pie chart, which shows major minerals and groups including carbonates, sulfides and accessory minerals. Theouter ring then shows a more detailed version, with every mineral measured (i.e., carbonates are broken down into calcite, ankerite, dolomite; sulfides are broken down into pyrite, chalcopyrite, etc). Abundant minerals are annotated onto the pie charts, and a key for all of the colours is along the bottom. Note these colours are not the same as those on the mineral map.

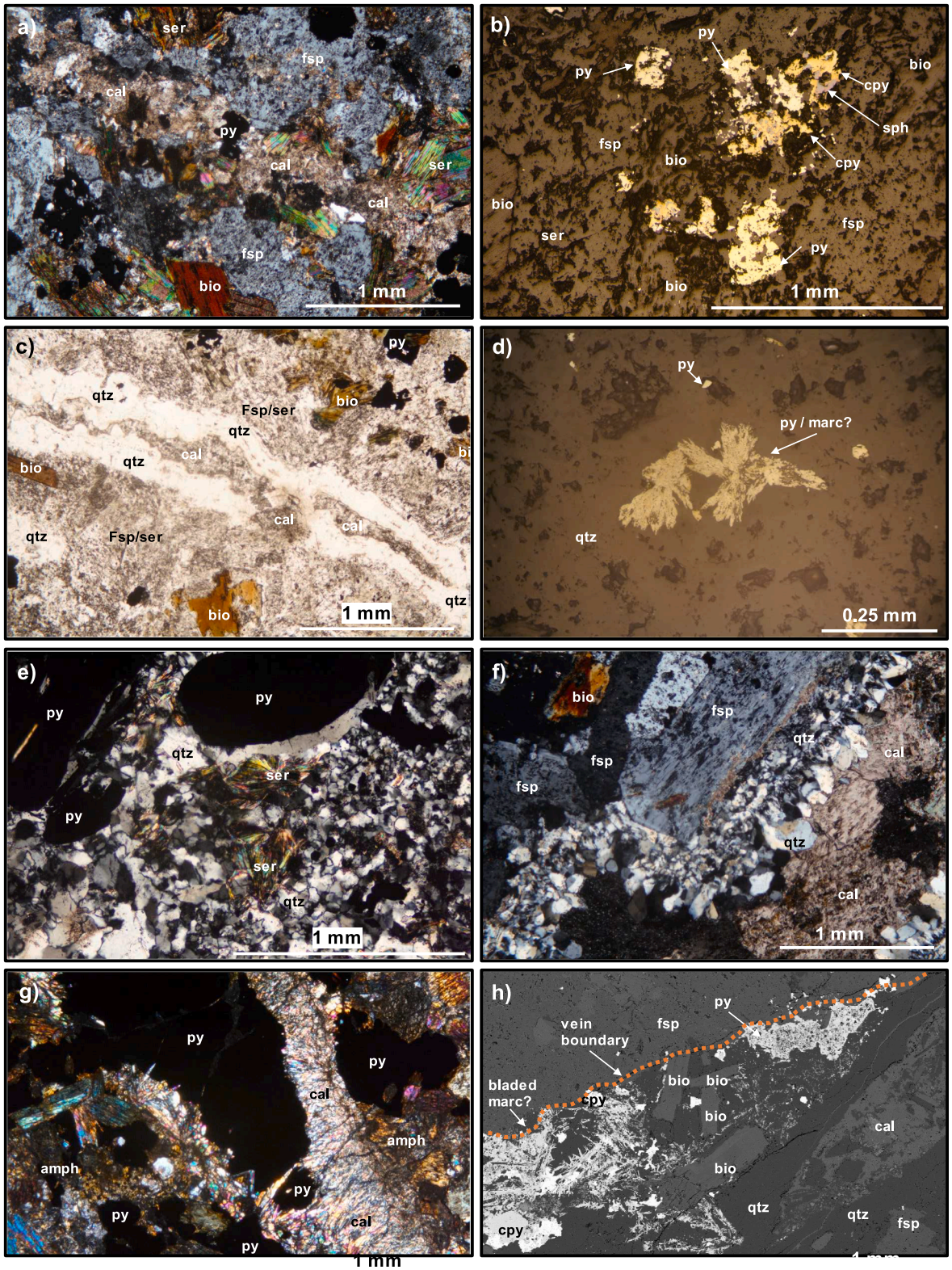

Fig. 5. A) tl photomicrograph in xpl showing a thin calcite (cal) stringer cutting through alteration assemblage including biotite (bio), sericite (ser) and blebby sulfides; b) rl photomicrograph showing porous chalcopyrite (cpy) and sphalerite (sph) with porous, previosuly euhedral pyrite (pyr); c) tl photomicrograph in ppl showing a veinlet lined with quartz (qtz) and infilled with calcite; d) rl photomicrograph showing bladed pyrite / marcasite (marc) in a quartz vein; e) tl photomicrograph in xpl showing an area of quartz dominated alteration, with blebs of pyrite and acicular fans of sericite; f) tl photomicrograph in xpl showing the edge of a quartz vein showing banded comb textures, infilled with massive calcite and adjacent to coarse sanidine crystals; g) tl photomicrograph in xpl showing a coarse calcite vein in heavily altered rock, surrounded by amphibole and cutting corase pyrite crystals; and h) bse image showing the distinct boundary between a quartz and calcite filled vein, with overgrowing biotite, bladed marcasite, porous pyrite and euhedral chalcopyrite.

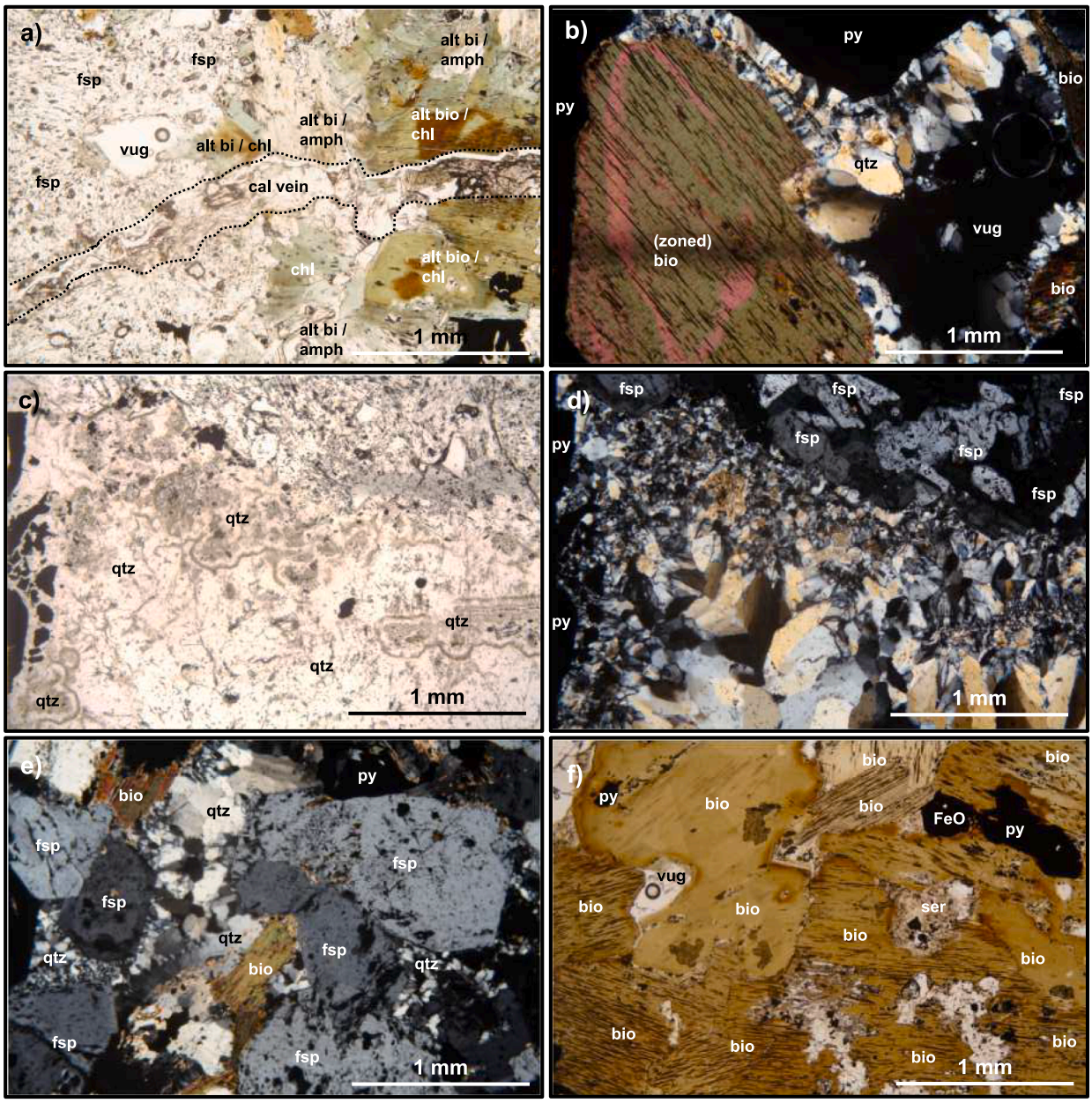

Fig. 6. A) tl photomicrograph in ppl showing a relatively rare calcite (cal) veinlet with no associated ore minerals and in association with heavily altered biotites (bi), feldspars (fsp) and amphibole (amph) and vugs; b) tl photomicropgraph in xpl showing a coarse zoned biotite next to vug filling quartz (qtz) and large euhedral pyrites (pyr); c) tl photomicrograph in ppl showing colloform quartz textures transitioning to massive / comb quartz and lined with broken pyrite crystals; d) tl photomicrograph in xpl of the same view as in c), illustrating the sharp boundary between feldspars and quartz and the increasing crystal size of quartz towards the ventre of the vug; e) tl photomicropgraph in xpl showing coarse, relatively unaltered feldspar crystals, altered biotites and fine-grained mosaic quartz filling angular vugs; and f) tl photomicrograph in ppl illustrating the abundance of coarse biotites in sections with sericite, pyrite and iron oxide (feo) overgrowths.

a few centimetres of vein margins (Fig. 2 a, Fig. 3 a and b). Like the veins, selvages commonly have a well-defined boundary. Oxides are increasingly abundant with proximity to mineralised rocks, as are disseminated pyrites. Alteration assemblages vary within the same lode and the same lode group. Differences between selvages are illustrated in Fig. 3. Paler selvages are composed of alkali feldspar, sericite, epidote, and other white clays, though some also contain pervasive quartz and, more rarely, carbonate (e.g., Fig. 3 c and g). Pale selvages therefore reflect potassic, sericitic, and propylitic alteration. The latter is variably developed with some assemblages containing epidote in addition to chlorite and sericite (e.g., Fig. 3 e). Darker selvages (e.g., Fig. 3 d and h) contain hydrothermal biotite, chlorite, and occasionally minor disseminated sulfides, primarily pyrite. In some cases, selvages are zoned, transitioning from biotite-dominated, to sericitic or propylitic alteration, to host rock. Close to veins but outside of selvages, coarse (<5 mm) apple-green epidote crystals and tabular sanidines can locally be observed at the hand specimen scale. Different domains of alteration observed in drill core also include 'green-rock' and 'pink-rock' alteration; the first being dominated by chlorite, epidote, and green micas, and the second potassium-feldspars.

4.1.2. *HT Zone*

Alteration within the HT Zone is stronger and more extensive, with examples of over 5 m intervals of drill core being bleached (e.g., Fig. 2 a). Many samples are dominated by quartz, sericite, and potassium feldspars with others overprinted with coarse, shreddy biotites, up to 3 cm in length, and in some cases comprising >50% of area. Carbonate is rarer, and totally absent in some samples.

Table 2
The average % of thin section composed of the most abundant sulfide minerals in the deposit as a whole and within the Main versus HT zones. These values are based on the modal scan, which provided mineralogical mapping of full thin sections at a coarser scale (30x30 μm pixel size).

	Pyrite	Chalcopyrite	Galena	Sphalerite	Arsenopyrite	Covellite	Bornite
Whole deposit	4.88	0.17	0.12	0.04	0.02	0.005	0.0007
Main body	3.19	0.15	0.14	0.06	0.03	0.005	0.00009
HT Zone	9.53	0.20	0.06	0.0003	0	0.005	0.002

4.2. Quantitative mineralogy of drill core material

Lode petrology and mineralogy is described here with qualitative data from optical microscopy, hand samples, and core logging along with quantitative data from a subset of samples analysed using Mineralogic. These new quantitative data allows determination of modal compositions of mineralised material (including alteration and gangue minerals). Eleven samples across the Main Zone from lodes were scanned: three SKL, three Murau, one GRF, one Snake, and three UR samples. Locations range from depths of 10 to 300 m. Four samples from across the HT Zone were analysed, from depths ranging 15–85 m.

Modal mineralogical compositions of thin sections are illustrated in Fig. 4, showing normalised bulk compositions of each sample. Precious- and semi-metal phases (Au-Ag-Te-Se-bearing) were rarely identified at this resolution (step size = 35 μm), and on average constitute only 0.04 % area. However, bulk compositions capture differences in vein composition and alteration assemblages well.

4.2.1. Main Zone

Most samples are dominated by potassium feldspar; in combination with plagioclase and biotite, these three minerals typically make up >75% by area (Fig. 4). Proportions of each are variable, ranging between 10.8 and 70.3% for K-feldspar, 0.4–23.3% for plagioclase, and 0.8–16.3% for biotite, with mean proportions of 52%, 13%, and 11% respectively. This includes primary and hydrothermal phases of these minerals, the latter of which is associated with mineralisation. These are not quantitatively distinguished from each other in Mineralogic. All samples contain quartz and carbonates, the latter of which is usually calcite. Ankerite and dolomite are present in much lesser quantities (1.7% and 0.07% average by area respectively, compared to 4.4% for calcite – note that ankerite is skewed by one sample containing ~13%).

4.2.2. HT Zone

Samples from the HT Zone contain a large amount of potassium feldspar and biotite (similar to the Main Zone), with proportions ranging 30–75% (with an average of 54%) and 1–55% (with an average of 19%) respectively (Fig. 4). Plagioclase is less abundant and except for one sample with as much 12%, most have negligible amounts (average of 0.1%). Quartz is the dominant gangue phase but variable, ranging from 1.3 to 21.6%. Carbonates occur in much lower proportions, with an average combined total of 0.66% by area; calcite is dominant, followed by ankerite and dolomite.

4.2.3. Accessory phases

Amphibole (4.0% as opposed to 0.4%), epidote (0.17% as opposed to 0.001%), iron-oxide (1.1% as opposed to 0.12%), and roscoelite are more abundant in the Main Zone compared to the HT Zone. Apatite is much more abundant in the HT Zone with an average of 3 % by area compared to 0.8%, as is titanium-bearing iron oxide. Schreyerite, a vanadium oxide, was only measured (albeit in tiny quantities) across three of the four HT samples. The other V-bearing mineral identified was karelianite, identified in the Main Zone. Chlorite, rutile, thorite, and zircon are present in comparable proportions across both zones.

4.3. Mineralisation styles, textures, and mineralogy

4.3.1. Main Zone

The Main Zones consist of veins composed of quartz, calcite, minor feldspar, and pyrite. Veins are commonly lined with colloform, banded, and mosaic quartz, and infilled with calcite (Fig. 5). On a finer scale, quartz textures can be zoned, transitioning from one texture to another. Calcite is often massive, and less associated with sulfides, though some precious-metal mineralisation does occur within calcite veins. Vein fill may include feldspar, biotite, and sulfides.

Minor variations within individual lodes and within lode groups are present, mainly with regards to differing proportions of the same minerals, as opposed to differences in the minerals present. Mineral proportions show no correlation with depth, location, or lode type. They may reflect variations in vein thickness or may be a consequence of variable selvages and alteration styles. Differences between lode groups also show no correlation with depth or location, nor is there any correlation between different lode groups (Fig. 4).

4.3.2. HT Zone

In comparison to the thin veins that characterise the Main Zone, the HT Zone displays wider veins of quartz and pyrite, with coarse biotites and sulfides, and occasionally abundant magnetite. Differences between modal compositions include far less calcite in HT Zone compared to the Main Zone and more abundant quartz, which is more commonly banded or colloform. Spheres of quartz were also identified. The HT Zone commonly has a bleached, vuggy host rock.

Overall, similar to within the Main Zone, differences between modal mineral proportions are relatively minor. Whilst modal proportions of K feldspar, biotite, and pyrite across the Main Zone and HT Zone can be similar, the textures are entirely different. As opposed to small laths of primary biotite and hydrothermal biotites limited to selvages recorded in the Main Zone, those in the HT Zone are coarse and associated with quartz, large apatites grains (<6 mm), chalcopyrite, and minor carbonate. Pyrite is coarse and disseminated. Typical textures are shown in Fig. 6; note especially the much coarser grain size (and scale). Differences within the HT Zone include minor distinctions between the H and T lodes, and minor variations within the same lode. Compared to T lodes, H lodes appear to contain less magnetite, apatite, and biotite. Within T lodes, differences include variable proportions of biotite and sulfides.

4.4. Base metal sulfide composition and mineralogy

Table 2 shows the sulfide contents measured on Mineralogic. Pyrite, chalcopyrite, and galena are common at Tuvatu, with uncommon sphalerite. Chalcopyrite is the second most common sulfide, despite alkalic-hosted epithermal gold deposits generally containing more pyrite, sphalerite, and galena than chalcopyrite (Jensen & Barton, 2000). Gold assays >2 g/t from Tuvatu have a median S content of 1.8 wt%, indicating a modal sulfide content of <4 %, assuming a typical assemblage comprising pyrite, chalcopyrite, galena, and sphalerite.. Other Cu-bearing sulfides identified include covellite and bornite. Other sulfides present include arsenopyrite, and some pyrite grains have relatively high arsenic contents.

Whilst relative abundances of sulfide minerals are consistent across the Main Zone and the HT Zone, lodes in the latter are characterised by a higher absolute abundance of sulfide minerals. The average area composed of sulfides across the Main Zone is 5.2%; for the HT Zone, average thin section area was 9.8%. Of the 20 samples studied in-depth optically from the Main Zone, 16 contained sulfides visible at the microscope scale (80%), compared to nine out of ten from the HT Zone

Table 3
Table of precious- and semi- metal phases found within the samples on the SEM. Relative abundance in the two ore zones are represented by ticks (✓= relatively low abundance, ✓✓= relatively moderately abundant, ✓✓✓= relatively very abundant). Average area % is the average area % of bright phases and haloes mapped across all thin sections. Note statistics do not include grains where multiple phases were present, but boundaries were indistinguishable. However, these associations are noted in the common associations column and insight is included within text.

Precious- & semi-metal phase	Main Zone	HT Zone	Number of grains	Number of samples	Total area (μm^2)	Mean grain size (μm^2)	Median grain size (μm^2)	Common associations
Native-Au (100 % Au)	✓✓	✓	112	14	618	5.5	0.7	Predominantly pyrite and quartz, lesser arsenopyrite, calcite, amphibole, and potassium feldspar; minor plagioclase, biotite, galena, and sphalerite.
Au-Ag alloy	✓	✓	18	8	49	2.7	1.4	No dominant associations; those noted include amphibole, plagioclase, calcite, biotite, potassium feldspar, and pyrite.
Calaverite (AuTe)	✓✓✓	✓	472	6	9603	20	5.4	83 % of grains at least partially touching quartz; otherwise associated with roscoelite, pyrite, and potassium feldspar.
Petzite (Ag_3AuTe_2)	✓✓✓	✓✓	248	10	6164	25	9.5	Within quartz and calcite veins, some association with roscoelite and potassium feldspar plus chalcopyrite, sphalerite, minor calaverite and Au-Ag alloy. < 20 % show any association with pyrite
Krennerite (Au_3AgTe_8)	✓✓	✓	8	2	120	15	7.8	Quartz and roscoelite
Sylvanite ((Ag, Au)Te_2)	✓	✓	16	2	89	5.5	1.4	13/16 enclosed in pyrite, others on edge of quartz vein
Hessite (Ag_2Te)	✓✓	✓	135	8	1005	7.5	2.1	Dominantly enclosed in or associated with pyrite, chalcopyrite, minor sphalerite, and quartz
Empressite (AgTe)	✓✓	✓✓	165	9	930	5.6	2.1	Dominantly enclosed in or associated with pyrite and chalcopyrite, some association with quartz and roscoelite
Stützite (Ag_7Te_4)	✓✓	✓	76	4	170	2.2	1.4	Mostly found enclosed in pyrite, with some on edge of quartz vein
PdPtTe	✓	✓	13	3	75	5.8	3.4	Associated with pyrite, quartz, calcite and chalcopyrite
PtTe	✓	–	5	3	5.6	1.2	0.7	Associated with quartz, pyrite, calaverite and altaite
CuTe	✓	✓	7	4	33	4.1	0.7	Mainly associated with pyrite
BiTe	✓	–	4	2	19	4.8	2.7	All associated with silicates: 3 with biotite and 1 with potassium feldspar
Altaite (PbTe)	✓✓✓	✓	1044	10	11,200	10.7	2.2	Mostly hosted within pyrite, but some associated with chalcopyrite, and some within quartz veins in association with potassium feldspar
Coloradoite (HgTe)	✓✓	✓	72	7	281	3.9	1.4	Hosted within and between potassium feldspar, quartz and pyrite
Ag-Cu-Te-S phase	✓✓	–	32	1	1071	33	17.5	Mostly associated with quartz. Variable proportions.

(90%). Four of the nine HT lode thin sections showing sulfides contain coarse (>3 mm) crystals.

4.5. Precious- and semi-metal mineral composition and mineralogy

A brief description of precious- and semi-metal bearing phases is displayed in Table 3, and relative compositions, along with total area of all precious- and semi-metal phases as measured during the bright phase search, are shown for each thin section in Fig. 7.

Gold is the primary economic metal at Tuvatu, present as native Au, Au-Ag alloy, and tellurides. Grades in assayed intervals range into the hundreds of ppm, though grain sizes are fine for most Au-rich phases. Native Au is found as 112 grains across 14 of the 15 samples. The average size is just 5.5 μm^2, with a range of < 1–112 μm^2, and particles are usually rounded. Only 18 grains of Au-Ag alloy were identified. The range of Au-Ag ratios of all grains is 42% to 99% Au, with the mean and median being 76% and 81% respectively. It is important to note the prevalence of native Au compared to Au-Ag alloy; when combining the two, Au grains have ultra-high fineness, with a mean and median Au content of 96.7% and 100% respectively. There appears to be no systematic variation in Ag content with grain size or mineral association. Metallurgical work by Lion One suggests that <10% of Au is bound in solid solution; total Au remains underestimated in SEM analysis as a consequence.

Although only 6 of the 15 samples analysed (across both zones, from lode groups SKL, UR, and T) contain calaverite, it is more abundant than native-Au and Au-Ag alloy by number of grains and has a larger average grain size, resulting in calaverite dominating Au deportment in the samples analysed. Nearly 3x as much Au by weight is measured in calaverite than in native-Au and Au-Ag alloy collectively. This is in line with an assessment by Bureau Veritas Commodities Canada ltd (2018), as outlined in the 2020 PEA for Lion One: based on one composite sample, calaverite dominated Au deportment, making up 81% by mass and 70% by mineral occurrences.

Petzite, krennerite, and sylvanite also contain Au, though the latter two are Ag-rich. Where present, Au-Ag-tellurides are associated with Ag-tellurides as opposed to Au-tellurides. These Ag-tellurides have compositions spanning empressite (AgTe; the most abundant by number of grains), hessite (Ag_2Te; the most abundant by area), and stützite (Ag_7Te_4). They make up a notable portion of four shallow samples (220–130 m reduced level (RL)) spanning different lodes (samples from Snake, UR2, and T1). Other precious-metal tellurides present include Pt-telluride, assumed to be moncheite ($PtTe_2$), and a Pd-(Pt)-telluride.

Altaite (PbTe) is the most common telluride at Tuvatu, dominating total number of phases and total area by an order of magnitude when compared to the second most common, calaverite. Altaite and calaverite are commonly associated, though this may be an artefact of their abundance. Coloradoite (HgTe) is also associated with altaite and calaverite, forming particularly on the rims of, or adjoined to, calaverite. Seven grains of Cu-telluride were observed within pyrites in multiple sections. Bismuth telluride was the rarest telluride species, with only four particles identified. In addition, a tellurosulfide phase, containing Ag and Cu was also observed. Although only in one sample, its grain size was relatively coarse, with a mean of 33 μm^2. Relative proportions varied between grains, and the SEM was not considered suitably accurate for stoichiometric analysis to suggest the mineral name.

4.5.1. Main Zone

All samples containing combined precious- and semi-metal phase

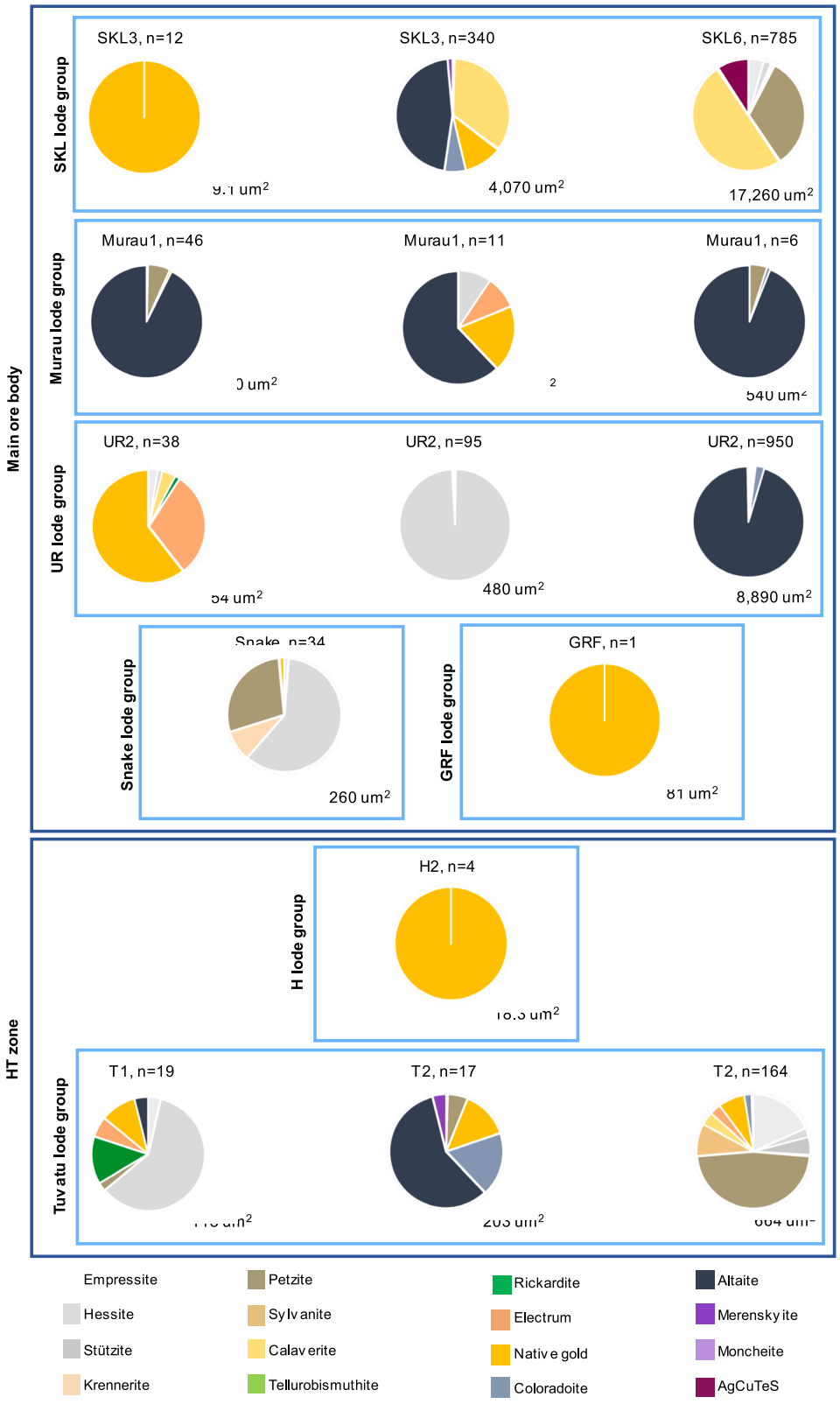

Fig. 7. Pie charts showing the precious- and semi-metal phase compositions of each thin section as identified during the bright phase search and detailed manually. Thin section name and lode hosted within the thin section is above each pie, along with total number of precious- and semi-metal phases identified. The total combined area of all precious- and semi-metal phases is shown to the bottom right of each pie. A key for all of the colours is along the bottom. Such pie charts ilustrate the abundance of Au- and Te- bearing minerals in different lodes across the Main Zone and the HT Zone.

areas of >1,000-μm come from the Main Zone, with two samples from SKL lodes, and one each from the UR and Murau lode groups. The three samples from Murau show the least variability in that all are dominated by altaite, but the absolute number and area of phases varies by two orders of magnitude. Two of the three samples from the SKL lodes have some of the highest total abundances of precious- and semi-metal, largest precious- and semi-metal phase area, and are dominated by calaverite, but aside from this they show little similarity. The UR2 samples also show no characteristic traits.

4.5.2. *HT Zone*

The number of grains of precious or semi-metals in the HT Zone is

Table 4
Table showing the relative % (by number of occurrence) of major phases which host or directly touch, and are therefore associated with, Au and Te bearing phases. Some totals may not add up to 100 due to rounding.

System	Mineral	Qtz	Carb	K-spar	Bi	Plag	Amph	*Epi*	Py	Asp	Gal	Sphal	Cpy	Cov	Rosc
Au-Ag	Native-Au	19	8	12	9	4	8	1	23	8	4	1	2	–	–
	Au-Ag alloy	9	9	–	9	9	27	–	32	–	–	–	–	–	–
Au-Te	Calaverite (AuTe)	70	–	9	0	1	0	–	12	–	–	0	1	–	11
Au-Ag-Te	Petzite (Ag_3AuTe_2)	48	9	–	–	–	–	–	15	–	–	3	5	–	17
	Krennerite (Au_3AgTe_8)	16	–	–	–	–	–	–	8	–	–	16	16	–	42
	Sylvanite ($(Ag,Au)Te_2$)	12	6	–	–	–	–	–	76	–	–	–	–	–	12
Ag-Te	Hessite (Ag_2Te)	30	1	–	1	–	–	–	56	–	–	8	7	1	3
	Empressite (AgTe)	23	–	–	–	–	–	–	50	–	–	4	11	2	16
	Stützite (Ag_7Te_4)	#	–	2	2	–	–	–	#	–	–	3	7	–	6
PGE- Te	PdPtTe	10	10	10	–	20	–	–	40	–	–	–	10	–	–
	PtTe	60	–	–	–	20	–	–	20	–	–	–	–	–	–
base metal - Te	CuTe	10	–	–	10	–	–	–	50	–	10	–	20	–	–
	BiTe	–	–	20	60	–	–	–	20	–	–	–	–	–	–
	Altaite (PbTe)	7	–	24	2	2	–	–	56	–	–	3	4	–	–
	Coloradoite (HgTe)	22	–	40	7	2	–	–	21	–	–	–	–	–	2
	Ag-Cu-Te-S phase	72	–	–	–	–	–	–	5	–	–	5	3	8	5

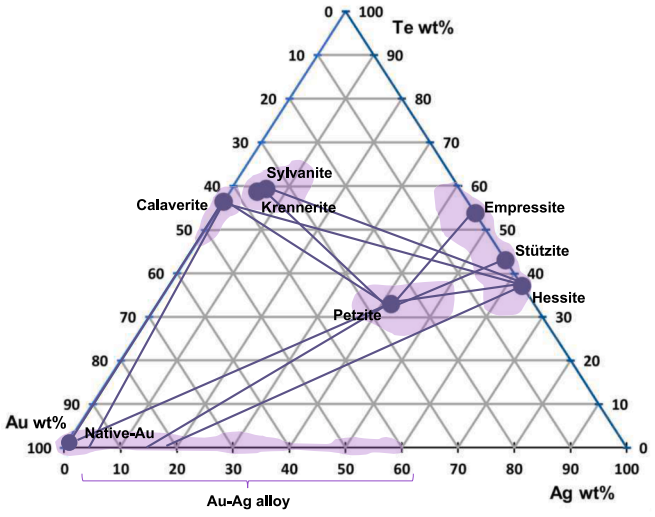

Fig. 8. Ternary plot of the Au-Ag-Te system, with ideal end-member compositions from Cabri (1965). Purple areas represent the variation in compositions for each mineral phase identified in this study. Lines represent contact assemblages observed in assemblages at Tuvatu. Contact assemblages have been used to aid in the refining of the paragenesis, and are helpful when trying to constrain the conditions of mineral formation as the mineral combinations are likely to require more specific conditions then just one mineral alone. (For interpretation of the references to colour in this figure legend, the reader is referred to the web version of this article.)

consistently lower, and none of the thin sections with combined precious- and semi-metal phase areas of >1,000-μm were from the HT Zone. The bright phase compositions show no characteristic trends, even when samples come from the same lode.

4.6. Au-Te mineral associations

Minerals associated with (i.e., hosting, adjacent to, or intergrown with) Au and Te bearing phases are illustrated in Table 4. Of vein-forming minerals, quartz hosts the highest proportion of telluride species. Carbonate minerals host some tellurides, especially Au tellurides, but this isn't as prevalent quartz-hosted telluride. The association of carbonates and tellurides is stronger in the Main Zone, where there is more carbonate present in general. Other important associated phases include potassium feldspar, plagioclase, and biotite. Although sulfides contribute <10% thin section area, over half of all precious- and semi-metal phases are associated with sulfide minerals. Pyrite dominates, likely due to its dominance amongst sulfide phases. Arsenian pyrite is not a common phase, though it does have a strong association with Au where present. Other important associated phases include roscoelite, which is intimately associated with Au and Ag tellurides.

4.7. Ore mineral assemblages and paragenetic sequence

In addition to the refined paragenesis, an updated list of coexisting phases and assemblages is presented, with those in the Au-Ag-Te system presented in Fig. 8. Although most grains identified were isolated, the following contact assemblages were observed. There are a number of examples of the Ag-Cu-tellurosulfide in contact with calaverite, petzite, hessite, empressite and altaite. Although a couple of grains of Pd-Pt-Te and Pt-tellurides were observed in contact with other tellurides, the majority of the observed grains were isolated. However, they were identified in the same vein and setting, associated with calaverite, coloradoite, and altaite.

A refined paragenesis for the mineralisation at Tuvatu is detailed in Fig. 9, which has been developed to build on the published paragenesis by Scherbarth and Spry (2006) and references therein. Key updates include a change in terminology for the initial 'porphyry' stage, and the inference that mineralisation at Tuvatu is due to evolution of a poorly-developed porphyry system. Previous analyses reference the phyllic and Au-mineralising stages together, but we split these into separate stages, based on the refined analysis of precious- and semi-metals and identification of new minerals.

Stage 1 is controlled by the final stages of monzonite crystallisation, referred to elsewhere as 'porphyry' mineralisation (Scherbarth & Spry, 2006). Stage 1 minerals are primarily coarse albite, orthoclase, biotite, and apatite, most prevalent in the HT Zone. Barren biotite and minor pyrite stringers commonly cut Stage 1 mineral assemblages. Stage 2 is defined by domains of pink rock containing coarse apatite, K-feldspar, and magnetite. Thicker, vuggy biotite and sulfide veins are associated with this stage, with wider veins occasionally cutting Stage 1 stringers and, in some cases, offsetting them. Rarer propylitic alteration, including abundant epidote, chlorite, actinolite, sericite, and muscovite is represented in Stage 3 and comprises phyllic-propylitic alteration, comprised of domains of green rock in drill core. Stage 2 and 3 are commonly spatially associated, although this is not exclusive. Neither show any clear spatial relationship to precious- or semi-metal mineralisation.

Ore mineralisation begins during Stage 4, termed the phyllic-sulfide-gold mineralisation stage, during which quartz, sericite, pyrite, and other sulfides overprint earlier stages, accompanied by minor Au. Most sulfides are deposited during this time. The Stage 4 Au is typically hosted

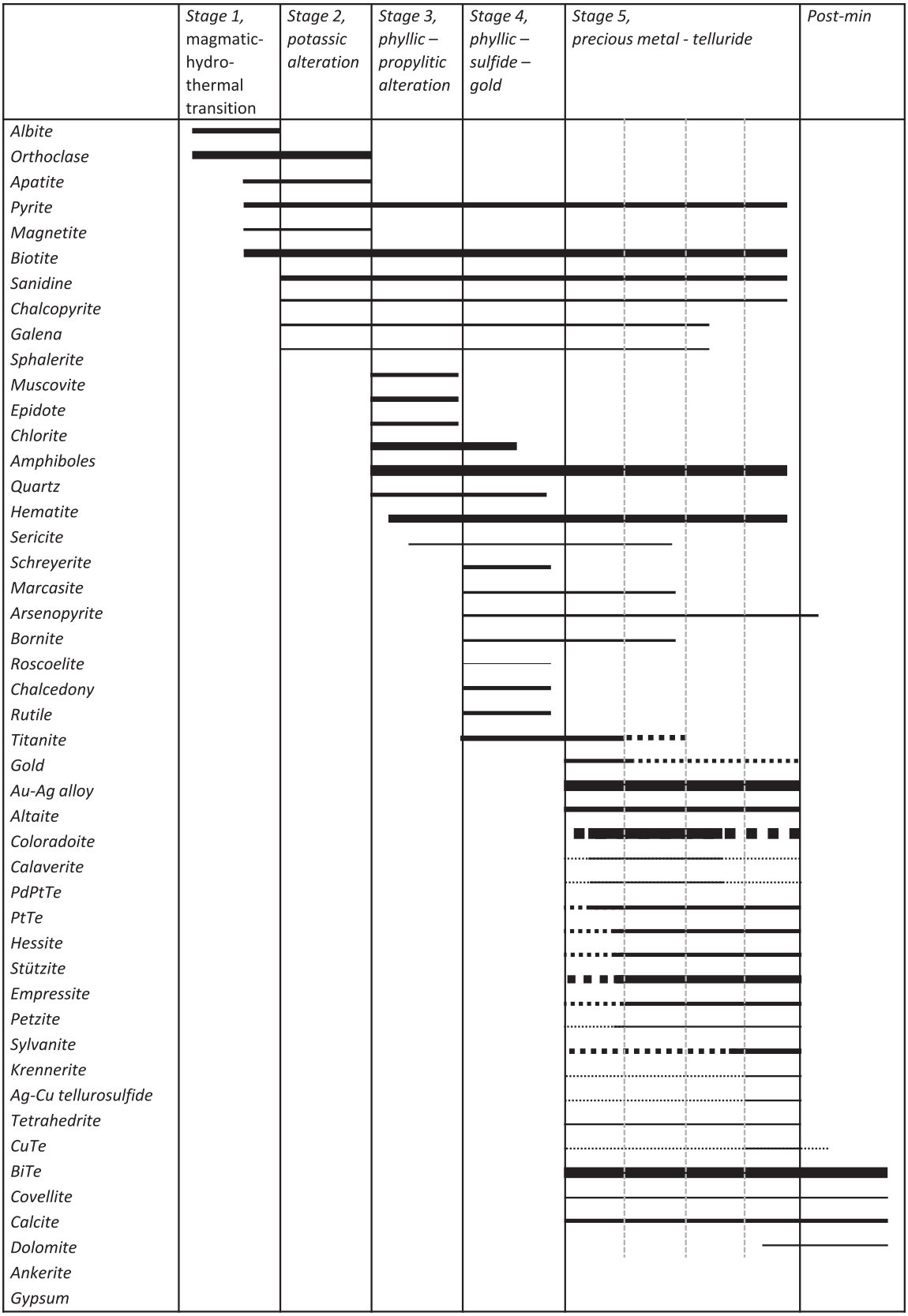

Fig. 9. Refined paragenetic sequence for the mineralogy of Tuvatu based on the new phases identified in this study, from Stage 1 to Stage 5. Stage 5 is broken into 4 sub-categories as outlined in the text (5a through to 5d), upon the assumption that these sub-stages are a result of time – though this is not definitive. Post-min refers to alteration minerals which overprint and post-date ore-forming mineralisation. The thickness of the horizontal lines corresponds to relative abundance of the mineral as observed through microscopy. Some minerals identified in previous paragenesis of Tuvatu were not identified during this study and are therefore not in this version.

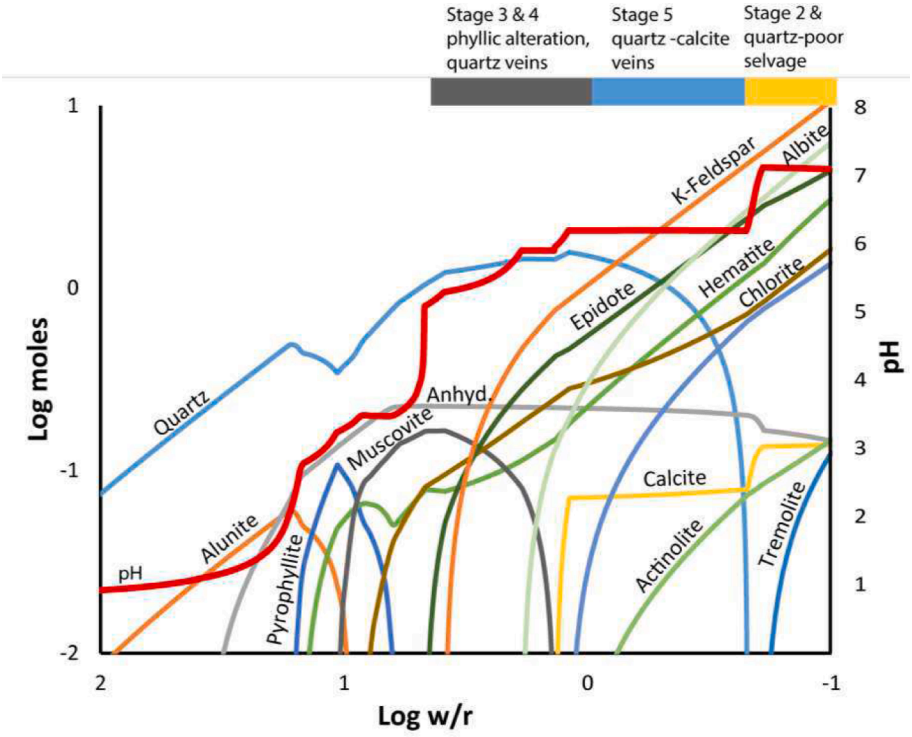

Fig. 10. Graph shows pH and log moles precipitated of major minerals during water rock reaction between monzonite and an idealised hydrothermal fluid at 300 °C. Some minor minerals have been omitted. X axis shows log water/rock, whereby the left side shows fluid-buffered conditions, and the right side shows rock-buffered conditions. Acidic, strongly fluid buffered conditions are not observed at Tuvatu, or indeed in any alkalic systems. Similar to the paragenesis, there's no single axis, and this graph can be read in terms of time, flux, depth, and can represent veins and selvage. Nevertheless, different parts of the paragenesis map well onto quartz, calcite, and tellurides, whereby acidic conditions precipitates quartz, gold, and no calcite; neutral conditions produce quartz, calcite, and tellurides; and alkaline conditions precipitate carbonates, with no quartz, and Au and Te in solution.

within sulfides or quartz veins, is ultra-high fineness, and is found independent to other ore phases, in samples that lack other ore minerals. Stage 5 'precious-metal telluride mineralisation', is divided into four separate assemblages. Generally, this stage includes epithermal-style mineralisation dominated by quartz, with lesser carbonates and feldspars. The presence of high fineness native-Au, in the same samples as but spatially removed from Ag-rich Au-Ag-tellurides may be suggestive of different phases. Furthermore, Pt- and Pd-Pt-tellurides occur in close proximity to calaverite but not Ag-tellurides, and no Ag-Pt-tellurides were identified, further suggesting separate phases. Finally, the abundance of a coarse, blebby Cu-Ag-tellurosulfide in only one sample, associated with tetrahedrite and covellite suggests a final phase.

Associations between minerals suggest four separate Stage 5 assemblages:

5a) Native-Au, auriferous electrum, and minor calaverite, interstitial to quartz and other minerals, although also hosted within quartz and minor calcite veins, or, most rarely, within pyrite, arsenopyrite and galena. Both altaite and coloradoite have been identified in contact with native-Au, so are interpreted to have begun deposition by this stage.

5b) Dominant calaverite, associated with minor hessite, petzite, Pt- and Pd-Pt-tellurides. These are hosted within or on the edges of quartz, roscoelite, and calcite grains, and less often within pyrite. This assemblage is found primarily in samples occurring at around 150 m RL.

5c) Ag-tellurides, including empressite, hessite and stützite, alongside lesser petzite and Ag-rich sylvanite, preferentially hosted within sulfides. This assemblage is notable across different lode groups but is principally in samples between 220 and 130 m RL (i.e., above 5b, and therefore shallower).

5d) Cu-Ag-tellurosulfide, along with Ag-tellurides, including empressite, hessite and stützite, and lesser petzite, associated with chalcopyrite, sphalerite, tetrahedrite, and covellite. This was observed in only one sample.

Altaite and coloradoite are not restricted to any one assemblage. Despite being the most abundant telluride, altaite usually occurs enclosed in pyrite, so its timing within these groups is difficult to determine. Bismuth telluride occurs exclusively in biotite, so is difficult to constrain to a stage. Post-mineralisation calcite veining was logged in abundance, and gypsum is also associated with this very final stage. Overall, where multiple assemblages are found in one sample, they appear independently and show different associations, but direct relationships are difficult to ascertain. Rarely, Ag-tellurides were found in calcite veins cutting coarse calaverite grains, though no abundant cross-cutting relationships between these groups were identified to confirm any sequence. In keeping with this, it has been stated elsewhere that Au-tellurides were deposited first, followed by Ag-tellurides (Spry & Scherbarth, 2006), though it should be noted that calcite veins cutting calaverite do also contain some Au-bearing tellurides.

Following Stage 1 and during periods of cooling and mineralisation, two deformational events occurred (A-Izzeddin, 1998). These include D1, the formation of the Core Shed Fault, and D2, which formed the CABX reverse fault, the various north, north-east, and northwest trending structures, and the subvertical structures, the latter two of which supply the main sites for ore deposition. Minor brecciation is observed in some veins, which may support structures being active during vein deposition. The prevalence of carbonate in veins and in faults may support this, though carbonate does exploit quartz veins formed previously.

5. Discussion

5.1. Nature of ore and deposit classification

Mineralisation at Tuvatu can be split into two styles: the high-grade Main Zone composed of thin stringers of dominantly precious and semi-metal phases (Fig. 5); and the lower-grade, relatively sulfide-rich HT Zone (Fig. 6). Within the Main Zone there is limited variability in modal (Fig. 4) and sulfide mineralogy between different samples, though the amount of, and mineralogy of Au-Te mineralogy varies greatly between samples (Fig. 7). This is a function of thin but extensive veins producing isolated and spotty mineralisation. Yet, within and between individual lodes and lode groups, there are no obviously systematic variations between lodes or laterally across the deposit (excepting the HT Zone).

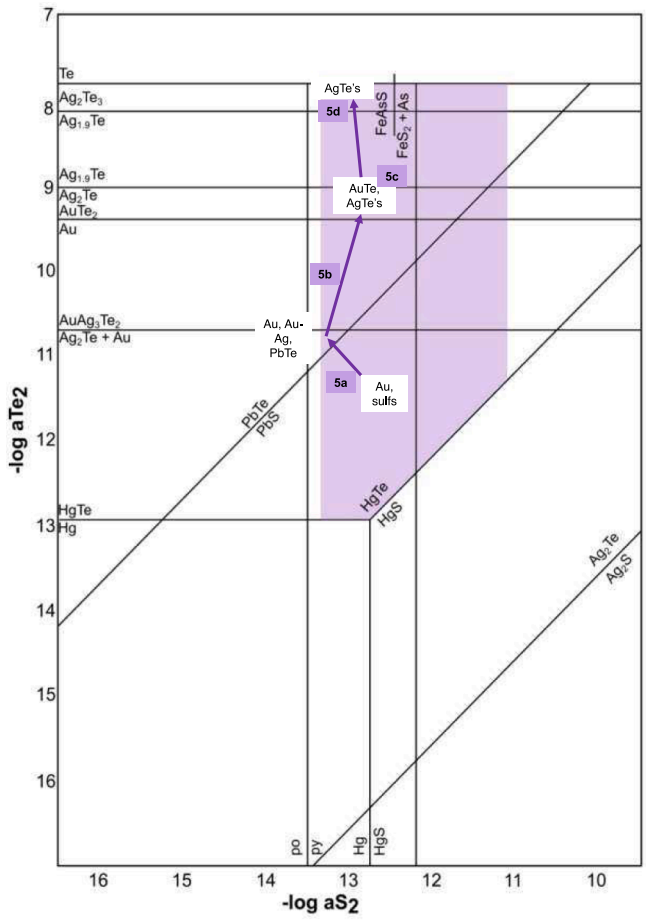

Fig. 11. Log a_{Te2} vs log a_{S2} diagram showing the relative stabilities of phases in the Te-S system at 250 °C, considering the metals Au, Ag, Pb, and Hg given they contribute the most common telluride phases. Cu and Bi are not included as they are not considered dominant phases. The purple shaded area is that of Scherbarth and Spry (2006), representing the approximate conditions for Stage 4 mineralisation in accordance with their paragenesis and their sphalerite analysis. (For interpretation of the references to colour in this figure legend, the reader is referred to the web version of this article.)

Gold grades at Tuvatu can be very high. This is common in alkalic-type epithermal deposits, which can be exceptionally Au-rich with high Te grades and tonnages compared to other low-sulfidation deposits associated with calc-alkaline igneous rocks (Jensen & Barton, 2000; Pals & Spry, 2003; Richards, 1995). Gold occurs as native gold (with very high fineness), and as precious metal tellurides (Table 3; Fig. 7). Multiple telluride species were identified, typical of alkalic-type epithermal Au deposits (Mutschler et al., 1985), and at Tuvatu there is some evidence of zonation with depth (e.g., occurrence of AuTe at approximately 150 m RL and Ag-tellurides above this at 220–130 m RL). Mapping of telluride phases at Vatukoula (Pals & Spry, 2003) and elsewhere (Kelley & Spry, 2016) shows telluride minerals are often unevenly distributed. Prior literature has suggested that invisible Au in pyrite makes a significant contribution (Scherbarth & Spry, 2006), with some as solid solution (Lion One Metals, 2015).

Other typical characteristics of alkalic-type epithermal deposits observed at Tuvatu include a base metal-poor assemblage (Table 2) and association with V-bearing minerals, including roscoelite (Table 4). Other V-bearing minerals identified during this study at Tuvatu include karelianite and schreyerite, and previous studies also identified an unnamed vanadian silicate (Spry & Scherbarth, 2006). Alteration at Tuvatu is dominated by epidote, sericite, sanidine, biotite, quartz, and carbonate, with little to no development of alteration assemblages related to acidic hydrothermal fluids (Fig. 3). Despite the association of quartz with mineralisation, alteration at Tuvatu rarely includes silicification or repeated generations of quartz-chalcedony veining that characterise many epithermal deposits, another common feature of alkalic-type epithermal mineralisation (Ciobanu et al., 2006; Jensen & Barton, 2000; Kelley & Spry, 2016; Kelley et al., 2020; Richards, 1995; Richards, 2009; Sillitoe, 2002). Despite differences between the HT Zone and the Main Zone, it is worth noting that many of the distinctive attributes of alkalic-type epithermal deposits are observed across both. Despite higher proportions of quartz, the HT Zone is not silicified. Multiple Au- and telluride phases were identified in samples across this area (Table 3), and Au/Ag, Au/Cu and Ag/Cu ratios are even higher than across the other lodes in the Main Zone.

For the first time at Tuvatu, Pt-Pd tellurides have been identified. An enrichment in Pt and Pd is highlighted in alkaline-related epithermal Au deposits elsewhere (Kelley & Spry, 2016; LeFort et al., 2011). In line with elsewhere, other PGE are not observed (Mutschler et al., 1985). In addition, we report a Cu-telluride phase, a Bi-telluride phase, and an Ag-Cu-tellurosulfide for the first time at Tuvatu (Table 3). Whilst Cu sulfides are more abundant than sphalerite, a trait uncommon in alkalic-hosted epithermal deposits, absolute abundances are still low. Despite nuances, Tuvatu is a typical alkalic-type epithermal Au deposit.

5.2. Genetic constraints for deposition

5.2.1. Modelled pH and mineral assemblages

The pH of the hydrothermal fluid was examined by modelling the titration of unaltered Tuvatu monzonite (TUDDH-437) into an initially acidic volcanic condensate at 300 °C (Reed, 1997; Smith et al., 2017). Iron oxidation state was recalculated to FeO + Fe_2O_3 by the method of Muller et al (2001). Modelling was carried out within CHILLER (Reed, 1982; Reed, 1998), and follows the design of the water–rock reactions of Reed (1997). The thermodynamic data used in the numerical experiments are from the database SOLTHERM.H08 (Reed et al., 2013). Data and calculations within SOLTHERM include: equilibrium constants calculated with SUPCRT92 (Johnson et al., 1992); mineral thermodynamic data for silicates, oxides, hydroxides, carbonates, gases (Holland & Powell, 1998) and sulphides (Shock, 2007). Mineral solid solutions are represented by end-member compositions that are mixed using an ideal multi-site mixing scheme.

Model results (Fig. 10) at high water/rock ratios are analogous to the conditions found in fluid-buffered hydrothermal systems, and low water/rock ratios represent rock-buffered conditions, as these are most likely to prevail in low sulphidation and alkalic type epithermal systems (Smith et al., 2017). Consistent with other alkalic-style Au deposits, the silica-undersaturated host rocks at Tuvatu support high pH fluids in rock-buffered conditions (pH 7 at 300 °C and log w/r − 0.7). Mineral assemblages show that quartz is absent from the alteration assemblage in rock-buffered conditions; the assemblage is feldspar, epidote, chlorite, calcite, and minor amphibole. Hematite seems to be over-represented (perhaps at the expense of pyrite and biotite) in the model results, suggesting that fluids were more reduced than those described elsewhere (Reed, 1997) and rocks less Fe^{3+}-rich than determined elsewhere (Müller et al., 2001).

Mineralisation at Tuvatu is related to quartz-bearing veins, yet compared to typical epithermal deposits, there is limited silicification and increased carbonation. Concurrent 'nebulous' alteration systems with subtle selvages, characterised by broad zones of potassic to sericitic alteration, are also typical. These characteristics are a function of the alkaline, silica-undersaturated rocks in which they are hosted in. As hydrothermal fluids interact with alkaline, silica-undersaturated host rocks, quartz is an equilibrium phase only at high water–rock ratios due to the flux of water through the volume of rock. Under rock-buffered conditions, quartz is absent or easily consumed by the system, enabling a high fluid pH (Smith et al., 2017). Pervasive alteration is therefore restricted to propylitic, sericitic, and (depending on

temperature) potassic-like assemblages, with massive silicification less likely.

A higher fluid pH may enhance the mobility of Te during hydrothermal alteration (Grundler et al., 2013; McPhail, 1994), including potentially enhanced leaching from host rocks. Precipitation of tellurides may occur in areas where quartz precipitates, as the quartz buffers the pH to <6 – and hence lower Te solubility (Smith et al., 2017). Lower pH, and quartz stability is achieved at higher water/rock conditions, in veins with higher fluid fluxes.

5.2.2. Textural constraints

Mineralisation is typically hosted within simple, parallel-sided, narrow veins, with little to no brecciation. There is minimal crosscutting of veins or lodes or complex overprinting events apart from Stage 4 native-Au and sulfide mineralisation being overprinted by Stage 5 mineralisation. Within veins, there is some evidence of changing mineralogy with vein evolution, with earlier quartz veins showing infills of carbonate (e.g., Fig. 5 c and f). There is limited evidence of veins being repeatedly exploited. Bladed calcite (or silicified equivalents) was not observed – but as noted in the previous section, calcite is likely to be stable in rock-buffered, high pH conditions, without boiling triggering rapid supersaturation (Fig. 10). (Moncada et al., 2012). Although the vein mineralogy at Tuvatu is similar to Au deposits within the epithermal family, Tuvatu lacks many of the characteristic vein textures of that class, such as botryoidal, colloform, banded, and bladed quartz. This suggests that mineralisation occurred as a result of the evolution of a single magmatic-hydrothermal system with relatively continuous fluid flux through veins. We suggest that the whole system is related to the emplacement, crystallisation, and cooling of the Navilawa Monzonite.

5.2.3. Mineralogical constraints

Maximum temperatures for hydrothermal telluride deposition are suggested to be ~354 °C, the melting point of hypogene sylvanite (Afifi et al., 1988); studies of other alkalic systems suggest that hypogene tellurides are deposited at temperatures between 300 and 100 °C (Kelley et al., 2020). Various mineralogical factors at Tuvatu suggest that temperatures remained on the higher end:

- Epidote is associated with all alteration assemblages and is indicative of temperatures > 250 °C (Eaton & Setterfield, 1993);
- Previous fluid inclusion work (Scherbarth & Spry, 2006), interpreted a mean temperature for Au mineralisation of ~ 250 °C;
- The presence of chalcopyrite and bornite also suggests high temperatures, especially given the dominance of the former over sphalerite.

5.2.4. Significance of Pd-Pt enrichments

In addition to Au and Te, PGE are recognised from alkalic porphyry-epithermal systems (Gonzalez-Jimenez et al., 2021; Hanley & MacKenzie, 2009; LeFort et al., 2011; McFall et al., 2018; Nixon & Archibald, 2001; Werle et al., 1984), and are uncommon in sub-alkaline-hosted equivalents (Kelley & Spry, 2016; Kelley et al., 2020). It is likely that the high partition coefficients of PGE into sulfides allow them to remain in subduction-associated cumulates until later remelting into post-subduction magmas, similarly to Au and Te (Richards, 2009). Enrichments of Pd and Pt (e.g., >100 ppb Pd) are suggested to be a function of alkaline magma formation (Kelley & Spry, 2016; Kelley et al., 2020; McFall et al., 2018), supported by many alkalic mineral deposits showing PGE enrichment (Holwell et al., 2019).

PGE-rich zones are common in alkalic-type epithermal Au deposits, though the presence of specific PGE-bearing phases in epithermal systems is uncommon (Kelley & Spry, 2016). At Tuvatu, Pd(-Pt) tellurides are present across multiple lodes, yet PGE are not routinely assayed to allow identification of enriched zones. An apparent lack of sopcheite, despite presence of Ag and Pt-tellurides, is suggested elsewhere to be evidence of phase or spatial separation, e.g., Skouries, where authors have suggested that Ag and PGE are transported separately or are temporally or spatially separate (McFall et al., 2018). This is unlikely at Tuvatu given that mineralisation is associated with one phase of magmatism, and both Ag- and Pt- tellurides occur in similar areas. Palladium- and Pt-tellurides are commonly considered higher-temperature phases. Where present, telluride melts <900 °C are thought to be responsible for Pd-Pt enrichments in upper crustal deposits, remaining as an immiscible liquid in the high temperature hydrothermal fluid down to ~400 °C (Gonzalez-Jimenez et al., 2021; Holwell et al., 2019; McFall et al., 2018). Only at temperatures >300 °C, in highly oxidising/acidic conditions, do Pd and Pt become significantly soluble in aqueous fluids (Wood et al., 1992), with temperatures >400 °C further increasing solubility (Tarkian et al., 2003). As outlined by pH indicators, the system is not highly acidic, suggesting temperature is the key driver.

5.2.5. Activity diagrams

Fig. 11 shows log a_{Te2} versus log a_{S2}, illustrating the stabilities of Te species at 250 °C. The re-estimation of values and evolution pathways on the graph are based on newly reported contact assemblages and subsequently revised paragenesis from this study. Previous work has suggested that temperature changes do not affect the topology of these diagrams, although absolute values change and some phases appear or disappear (Afifi et al., 1988). Whilst evolution pathways persist, absolute limits of (log) activity of $Te_{2(g)}$ at 250 °C to 100 °C change to between -14.1 and -21.5 respectively, whilst the lower S_2 activity based on the pyrrhotite-pyrite buffer decreases to -25 (Afifi et al., 1988). Regardless of temperature, trends in $Te_{2(g)}$ activity can be defined by observed assemblages and the presence or absence of specific minerals.

Across Tuvatu, $Te_{2(g)}$ activity appears to increase with time. The assemblage must sit within the field bound by a lack of pyrrhotite, whilst the upper limit of activity of $Te_{2(g)}$ is below the stability of native Te, given its absence. The lower limit of $Te_{2(g)}$ activity on Fig. 11 is defined by the presence of hessite (Afifi et al., 1988), however, given the presence of coloradoite rather than cinnabar or native mercury, we assume the HgTe dictates the lowest limit of $Te_{2(g)}$ activity at Tuvatu. Stages 5c and 5d contain Au-Ag tellurides, suggesting higher $Te_{2(g)}$ activity. Telluride mineralisation after initial sulfide deposition, such as the transition from Stage 4 to Stage 5b (Fig. 11), is thought to reflect an increase in f_{Te2}/f_{S2} – likely due to an input of H_2Te from a magmatic source (Afifi et al., 1988). This is shown by the transition from native-Au and sulfides, into Au deposition with PbTe and HgTe, and then to a calaverite-dominated assemblage with some Ag-tellurides.

5.2.6. Depth vs time

The main mineralisation stage, 'Stage 5′, shows evidence of zonation with depth, though the same evolution could be a function of time. Limited crosscutting relationships suggest that 5a formed prior to 5b and 5c, and it has been suggested that Au tellurides were deposited prior to Ag tellurides (Scherbarth & Spry, 2006). Paragenetic sequences of telluride deposition from various deposits suggest that generally, metal ratios control the order of deposition (Grundler et al., 2013); hence, Au-rich tellurides form first in deposits where bulk Au is high. However, samples with significant calaverite are found deeper than those dominated by Ag-tellurides (Ag tellurides at 220, 170, 165 and 130 m RL; calaverite at 145 and 150 m RL) Yet, it should be noted that these Ag-tellurides are found, albeit in lesser quantities, in deeper samples too. The transition between Stages 5a to 5d suggests an increase in f_{Te2} over time, or in the shallower parts of the deposit – a feature noted at other telluride-bearing systems and ascribed to boiling of fluids and mobilisation of Te-rich vapours (Börner et al., 2021; Cooke & McPhail, 2001; Keith et al., 2018).

5.3. Ore genesis model for Tuvatu

Despite the high Au grades observed at Tuvatu, there is no evidence of vein reactivation (except re-exploitation of veins by later calcite) or

extensive overprinting events. Within the veins, fluid flow results in higher water/rock (fluid-buffered) conditions, and hence decreases the pH, which reduces the solubility of Te and potentially Au (Smith et al., 2017), resulting in Au-(Ag)-telluride precipitation, typically accompanied by quartz. The simple veins indicate that mineralisation was monogenetic which, in order to deposit Au effectively, either requires a highly effective precipitation process, or a very long-lived system. The lack of strong pervasive alteration in the host would seem to preclude the latter. Instead, we suggest that boiling – as in many epithermal deposits – is a key process by which Tuvatu fluids precipitated precious metals in the veins effectively. Subtle evidence of boiling textures is found within quartz throughout the HT Zone, including crustiform quartz on vein edges, crustiform/banded quartz infilling vugs, and spheres of quartz (Moncada et al., 2012). We suggest that higher fluid pH in alkalic systems mean that "bladed calcite" and its pseudomorphs – a common indicator of fluid boiling in epithermal systems – are unlikely to form in deposits similar to Tuvatu, as calcite precipitation is the norm, rather than a solely boiling-induced process.

Boiling itself can cause the partitioning of elements into different fluid phases, and is considered to contribute to the distinct vapour and liquid phases at Tuvatu. Although boiling of a neutral to alkaline fluid can partition (retain) significant Te in the liquid phase, some Te is expected to partition into the vapour even in oxidising conditions (Grundler et al., 2013; Keith et al., 2018). In reducing conditions, at moderate to low fO_2, partitioning of Te is strongly into the vapour, where concentrations can reach > 100 ppm (Cooke & McPhail, 2001; Pudack et al., 2009; Wallier et al., 2006). Recent work mapping trace elements including Te in pyrites formed during distinct phases at Cripple Creek suggested that boiling partitioned Te in the vapour, decoupling Te and Au (Keith et al., 2020). At Tuvatu in particular, we view boiling as being the likely cause of partitioning of Te into vapour phases, though some is likely retained in a liquid – this is suggested to be a cause of the multiple fluid phases responsible for the multiple stages of mineralisation, especially 5a–c and 5d.

PGE have been shown to partition into low salinity 'contracted' vapour phases following boiling at Mt Milligan and in experimental work (LeFort et al., 2011; Pokrovski et al., 2008). Furthermore, Au may be transported in a soluble complex with Te in vapour (Cooke & McPhail, 2001; Grundler et al., 2013; Jensen & Barton, 2000; Larocque et al., 2008). The process could prime fluids for later deposition from separate phases, where a liquid phase is responsible for high-fineness native-Au of Stage 5a, and the vapour phase is able to carry Au, Pt, Pd, and Te as deposited in 5b. Condensation of Te-bearing volatiles may be important within alkalic-type epithermal systems and is suggested at deposits such as Cripple Creek (Keith et al., 2020). This may occur upon reaction with aqueous Au species and lead to vertically zoned mineralisation (Cooke & McPhail, 2001), for which there is some evidence at Tuvatu.

6. Conclusions

Detailed, quantitative mineralogical studies at Tuvatu, a post-subduction, alkalic-type epithermal deposit, has enabled us to effectively identify and characterise small quantities of μm-scale, obscure minerals, some of which have not been identified at Tuvatu before. Based on this, we have been able to present an updated description of mineralisation and a refined paragenesis of the deposit. This refined paragenesis includes the addition of multiple telluride minerals, a more detailed understanding of possible zonation and changing Au deportment, suggesting evolution from an assemblage dominated by native Au to one rich in precious-metal tellurides.

On a deposit scale, Tuvatu displays two main styles of mineralisation: the Main Zone, characterized by thin, laterally extensive veinlets containing Au, tellurides, quartz, and carbonate, and the HT Zone with coarser, vuggy veins and less carbonate but higher amounts of base-metal sulfides and quartz. Within those two blocks, multiple veins are grouped into lodes with similar structural trends that show little marked systematic differences in mineralogy. We concur with previous studies (Lion One Metals, 2015; Scherbarth & Spry, 2006; Spry & Scherbarth, 2006) that the HT Zone mineralisation likely represents a chronologically earlier and hotter period of deposition.

We suggest a monogenetic period of ore formation, with evolution of the ore-forming fluid from low to high Te activities. Distinct styles of precious and semi-metal mineralisation were identified even within the Main Zone, which may be a function of telluride zoning with depth and controlled by spatial conditions as opposed to temporal. Evidence of zoning is especially prevalent in tellurides, which are more susceptible to variations in deposition at low temperatures. More focused analysis is required to ensure that depth is the control, as opposed to fluid evolution with time, although both factors are likely to play a role.

Native-Au across the deposit has very high fineness, yet a large portion of Au deportment is within precious-metal tellurides, which are dominated by Au-tellurides, with a large portion of Au-Ag- and Ag-tellurides. For the first time at Tuvatu, Pt- and Pd-tellurides were identified, which are rare for epithermal deposits and likely suggest higher temperatures than typically observed for this class of deposit. Although there is little to no systematic mineralogical variation between lodes, there is some zonation of precious metal tellurides with depth, with silver tellurides in the shallower portions of the system.

Mineralisation is monogenetic, associated with one phase of magmatism and only one period of mineralisation rather than multiple periods of overprinting. It is thought to occur via relatively high temperature fluids fluxing through the vein systems, with some intervals of boiling and vapour separation. Precious metal deposition was likely enabled by boiling and associated desulfidation, aided by fluid focussing which allows lowering of pH.

Declaration of Competing Interest

The authors declare that they have no known competing financial interests or personal relationships that could have appeared to influence the work reported in this paper.

Data availability

The data is in the paper / supplementary material - anything else can be made available upon request.

Acknowledgments

Thanks to Lion One Metals Limited, who were extremely helpful in allowing access to and the collection of samples.

This PhD project is funded by NERC CENTA DTP, with extra funding from the BGS University Funding Initiative (Project S392) and the Natural Environment Research Council (UK) grant NE/M010848/1 in the Security of Supply of Minerals programme.

Author contributions

All authors contributed to the study conception and design. Material preparation, data collection, and data analysis were carried out, and the first draft of the manuscript was written, by Rose Clarke. All authors commented on previous versions of the manuscript and read and approved the final manuscript.

Appendix A

Brief descriptions of each thin section.

Appendix B

limitations to automated mineralogy and additional protocol (including Fig. 12).

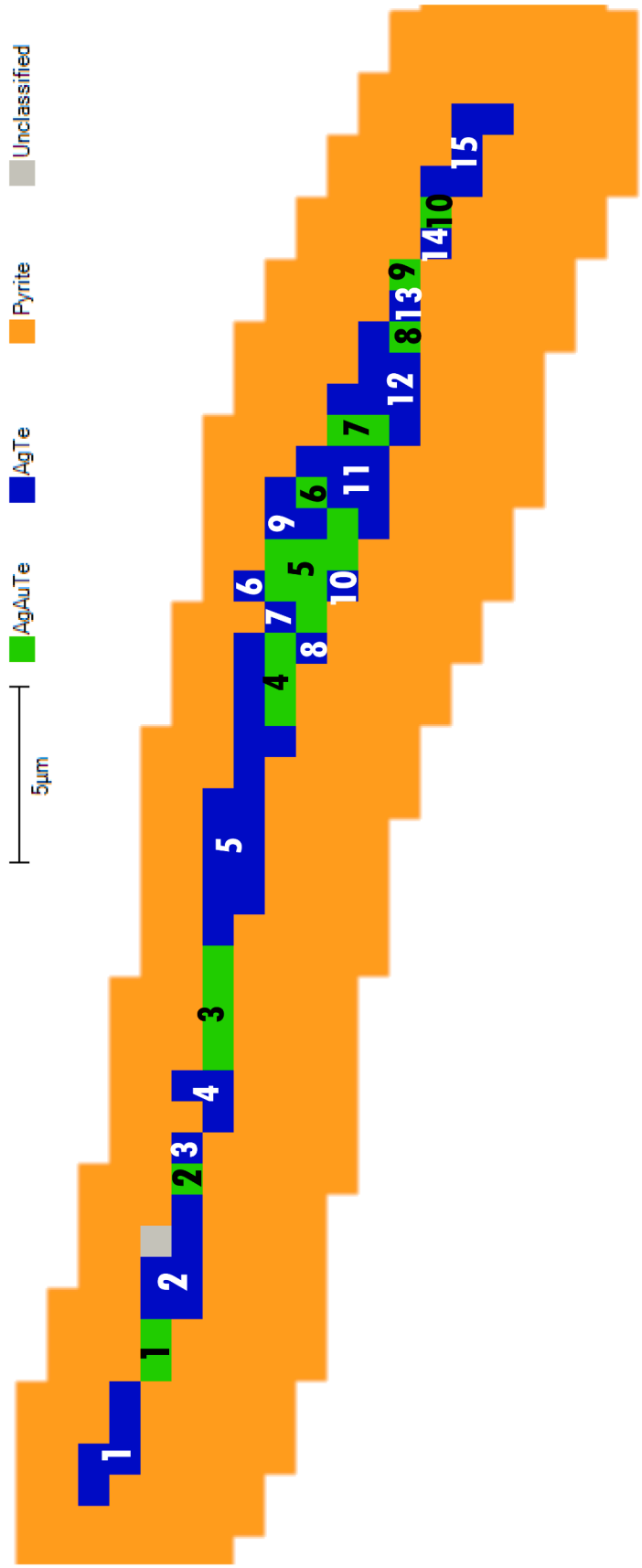

Fig. 12. Image of a grain of petzite mapped as different minerals on Mineralogic. Note Mineralogic measures this as 15 grains of AgTe and 10 grains AgAuTe, whereas this dataset considers it to be 1 grain of AgAuTe, more specifically petzite, given the prevalence of Ag.

Appendix C. Supplementary data

Supplementary data to this article can be found online at https://doi.org/10.1016/j.oregeorev.2022.105279.

References

Afifi, A.M., Kelly, W.C., Essene, E.J., 1988. Phase relations among tellurides, sulfides, and oxides; Pt. II, Applications to telluride-bearing ore deposits. Economic Geology and the Bulletin of the Society of Economic Geologists 83 (2), 395–404. https://doi.org/10.2113/gsecongeo.83.2.395.

A-Izzeddin, D. (1998). The Tuvatu gold project, western Viti Levu [Abstract]. *Pacific Exploration Technology (PET 98) Nadi, Fiji, September 1998, Abstract Volume,* 29-30.

Begg, G., Gray, D.R., 2002. Arc dynamics and tectonic history of Fiji based on stress and kinematic analysis of dikes and faults of the Tavua Volcano, Viti Levu Island. Fiji. *Tectonics* 21 (4), 5–14. https://doi.org/10.1029/2000TC001259.

Blanks, D.E., Holwell, D.A., Fiorentini, M.L., Moroni, M., Giuliani, A., Tassara, S., González-Jiménez, J.M., Boyce, A.J., Ferrari, E., 2020. Fluxing of mantle carbon as a physical agent for metallogenic fertilization of the crust. Nature Communications 11 (1), 4342. https://doi.org/10.1038/s41467-020-18157-6.

Börner, F., Keith, M., Smith, D.J., Barry, T.L., Neumann, T., Klemd, R., 2021. Fingerprinting fluid evolution by trace elements in epithermal pyrite, Vatukoula Au-Te deposit, Fiji. Ore Geology Reviews 137, 104314.

Ciobanu, C. L., Cook, N. J., & Spry, P. G. (2006). Preface – Special Issue: Telluride and selenide minerals in gold deposits – how and why? *Mineralogy and Petrology, 87*(3), 163-169. 10.1007/s00710-006-0133-9.

Clarke, R., Smith, D., Naden, J., 2022. Source controls on mineralisation: Regional geology and magmatic evolution of Fiji. Lithos 432-433, 106897. https://doi.org/10.1016/j.lithos.2022.106897.

Colley, H., Hindle, W., 1984. Volcano-tectonic evolution of Fiji and adjoining marginal basins. Geological Society, London, Special Publications 16 (1), 151. https://doi.org/10.1144/GSL.SP.1984.016.01.11.

Cook, N.J., Ciobanu, C.L., Spry, P.G., Voudouris, P., 2009. Understanding gold-(silver)-telluride-(selenide). mineral 32 (4), 249–263.

Cooke, D.R., McPhail, D.C., 2001. Epithermal Au-Ag-Te Mineralization, Acupan, Baguio District, Philippines: Numerical Simulations of Mineral Deposition. Economic Geology 96, 109–131.

du Bray, E.A., 2017. Geochemical characteristics of igneous rocks associated with epithermal mineral deposits—a review. Ore Geology Reviews 80, 767–783.

Eaton, P.C., Setterfield, T.N., 1993. The Relationship between Epithermal and Porphyry Hydrothermal Systems within the Tavua Caldera. Fiji. 88, 1053–1083.

Forsythe, N., Spry, P., Thompson, M., 2019. Petrological and Mineralogical Aspects of Epithermal Low-Sulfidation Au- and Porphyry Cu-Style Mineralization, Navilawa Caldera. Fiji. *Geosciences* 9 (1), 42. https://doi.org/10.3390/geosciences9010042.

Gill, J., Whelan, P., 1989. Postsubduction ocean island alkali basalts in Fiji. Journal of Geophysical Research: Solid Earth 94 (B4), 4579–4588. https://doi.org/10.1029/JB094iB04p04579.

Gonzalez-Jimenez, J.M., Pina, R., Kerestedjian, T.N., Gervilla, F., Borrajo, I., Pablo, J.F., Proenza, J.A., Tornos, F., Roque, J., Nieto, F., 2021. Mechanisms for Pd-Au enrichment in porphyry-epithermal ores of the Elatsite deposit. Bulgaria. *Journal of Geochemical Exploration* 220, 106664. https://doi.org/10.1016/j.gexplo.2020.106664.

Grundler, P. V., Brugger, J., Etschmann, B. E., Helm, L., Liu, W., Spry, P. G., Tian, Y., Testemale, D., & Pring, A. (2013). Speciation of aqueous tellurium(IV) in hydrothermal solutions and vapors, and the role of oxidized tellurium species in Te transport and gold deposition. *Geochimica Et Cosmochimica Acta, 120*, 298-235. 10.1016/j.gca.2013.06.009.

Hanley, J.J., MacKenzie, M.K., 2009. Incorporation of platinum-group elements and cobalt into subsidiary pyrite in alkalic Cu-Au porphyry deposits: significant implications for precious metal distribution in felsic magmatic-hydrothermal systems [Abstract]. American Geophysical Union. Spring Meeting 2009, Abstract Id. V14A–03.

Hathway, B., 1993. The Nadi Basin: Neogene strike-slip faulting and sedimentation in a fragmented arc, western Viti Levu. Fiji. *Journal of the Geological Society* 150 (3), 563. https://doi.org/10.1144/gsjgs.150.3.0563.

Holland, T., Powell, R., 1998. An internally consistent thermodynamic data set for phases of petrological interest. Journal of Metamorphic Geology 16 (3), 309–343.

Holm, R.J., Tapster, S., Jelsma, H.A., Rosenbaum, G., Mark, D.F., 2019. Tectonic evolution and copper-gold metallogenesis of the Papua New Guinea and Solomon Islands region. Ore Geology Reviews 104, 208–226. https://doi.org/10.1016/j.oregeorev.2018.11.007.

Holwell, D. A., Fiorentini, M., McDonald, I., Lu, Y., Giuliani, A., Smith, D. J., Keith, M., & Locmelis, M. (2019). A metasomatized lithospheric mantle control on the metallogenic signature of post-subduction magmatism. *Nature Communications, 10* (1), 3511-10. 10.1038/s41467-019-11065-4.

Jensen, E.P., Barton, M.D., 2000. Gold Deposits Related to Alkaline Magmatism. SEG Reviews 13, 279–314.

Johnson, J.W., Oelkers, E.H., Helgeson, H.C., 1992. SUPCRT92: A software package for calculating the standard molal thermodynamic properties of minerals, gases, aqueous species, and reactions from 1 to 5000 bar and 0 to 1000 C. Computers & Geosciences 18 (7), 899–947.

Keith, M., Smith, D.J., Jenkin, G.R.T., Holwell, D.A., Dye, M.D., 2018. A review of Te and Se systematics in hydrothermal pyrite from precious metal deposits: Insights into ore-forming processes. Ore Geology Reviews 96, 269–282. https://doi.org/10.1016/j.oregeorev.2017.07.023.

Keith, M., Smith, D.J., Doyle, K., Holwell, D.A., Jenkin, G.R.T., Barry, T.L., Becker, J., Rampe, J., 2020. Pyrite chemistry: A new window into Au-Te ore-forming processes in alkaline epithermal districts, Cripple Creek, Colorado. Geochimica Et Cosmochimica Acta 274, 172–191. https://doi.org/10.1016/j.gca.2020.01.056.

Kelley, K.D., Spry, P.G., 2016. Critical Elements in Alkaline Igneous Rock-Related Epithermal Gold Deposit. Reviews in Economic Geology 18, 195–216.

Kelley, K.D., Spry, P.G., McLemore, V.T., Fey, D.L., Anderson, E.D., 2020. Alkalic-Type Epithermal Gold Deposit Model Mineral Deposit Models for Resource Assessment. USGS.

Larocque, A.C.L., Stimac, J.A., Siebe, C., Greengrass, K., Chapman, R., Mejia, S.R., 2008. Deposition of a high-sulfidation Au assemblage from a magmatic volatile phase, Volcán Popocatépetl, Mexico. Journal of Volcanology and Geothermal Research 170 (1), 51–60. https://doi.org/10.1016/j.jvolgeores.2007.09.009.

LeFort, D., Hanley, J., Guillong, M., 2011. Subepithermal Au-Pd Mineralization Associated with an Alkalic Porphyry. Cu-Au Deposit, Mount Milligan, Quesnel Terrane, British Columbia, Canada. Economic Geology 106, 781–808.

Lion One Metals. (2015). *Tuvatu PEA NI-43-101*.

McFall, K.A., Naden, J., Roberts, S., Baker, T., Spratt, J., McDonald, I., 2018. Platinum-group minerals in the Skouries Cu-Au (Pd, Pt, Te) porphyry deposit. Ore Geology Reviews 99, 344–364. https://doi.org/10.1016/j.oregeorev.2018.06.014.

McPhail, D.C., 1994. Thermodynamic properties of aqueous tellurium species between 25 and 350°C. Geochimica Et Cosmochimica Acta 59 (5), 851–867.

Moncada, D., Mutchler, S., Nieto, A., Reynolds, T.J., Rimstidt, J.D., Bodnar, R.J., 2012. Mineral textures and fluid inclusion petrography of the epithermal Ag–Au deposits at Guanajuato, Mexico: Application to exploration. Journal of Geochemical Exploration 114, 20–35. https://doi.org/10.1016/j.gexplo.2011.12.001.

Müller, D., Franz, L., Herzig, P.M., Hunt, S., 2001. Potassic igneous rocks from the vicinity of epithermal gold mineralization, Lihir Island. Papua New Guinea. *Lithos* 57 (2–3), 163–186.

Mutschler, F.E., Griffin, M.E., Stevens, D.S., Shannon Jr, S.S., 1985. Precious metal deposits related to alkaline rocks in the north American Cordillera: an interpretive review. Verhandelinge Van Die Geologiese Vereniging Van Suid-Afrika 88 (2), 355–377.

Nixon, G.T., Archibald, D.A., 2001. Age of Platinum-Group-Element Mineralization in the Sappho Alkaline Complex. South-Central British Columbia.

Pals, D.W., Spry, P.G., 2003. Telluride mineralogy of the low-sulfidation epithermal Emperor gold deposit, Vatukoula. Fiji. *Mineralogy and Petrology* 79 (3), 285–307. https://doi.org/10.1007/s00710-003-0013-5.

Pokrovski, G.S., Borisova, A.Y., Harrichoury, J., 2008. The effect of sulfur on vapor–liquid fractionation of metals in hydrothermal systems. Earth and Planetary Science Letters 266 (3), 345–362. https://doi.org/10.1016/j.epsl.2007.11.023.

Pudack, C., Halter, W.E., Heinrich, C.A., Pettke, T., 2009. Evolution of Magmatic Vapor to Gold-Rich Epithermal Liquid: The Porphyry to Epithermal Transition at Nevados de Famatina, Northwest Argentina. Economic Geology 104 (4), 449–477, 0361-0128/09/3821/449-29.

Reed, M.H., 1982. Calculation of multicomponent chemical equilibria and reaction processes in systems involving minerals, gases and an aqueous phase. Geochimica Et Cosmochimica Acta 46 (4), 513–528.

Reed, M.H., 1997. Hydrothermal alteration and its relationship to ore fluid composition. Geochemistry of Hydrothermal Ore Deposits 303–365.

Reed, M.H., Rusk, B., Palandri, J., 2013. The Butte magmatic-hydrothermal system: One fluid yields all alteration and veins. Economic Geology 108 (6), 1379–1396.

Reed, M. H. (1998). Calculation of simultaneous chemical equilibria in aqueous-mineral-gas systems and its application to modeling hydrothermal processes.

Richards, J., 1995. Alkalic-type gold deposits: A review. *Magmas, Fluids and Ore Deposits, Mineral*. Assoc. Canada, Short Course 23, 367–400.

Richards, J., 2009. Postsubduction porphyry Cu-Au and epithermal Au deposits: Products of remelting of subduction-modified lithosphere. Geology 37 (3), 247–250. https://doi.org/10.1130/G25451A.1.

Rogers, N.W., Setterfield, T.N., 1994. Potassium and incompatible-element enrichment in shoshonitic lavas from the Tavua volcano. Fiji. *Chemical Geology* 118 (1), 43–62. https://doi.org/10.1016/0009-2541(94)90169-4.

Scherbarth, N.L., Spry, P.G., 2006. Mineralogical, Petrological, Stable Isotope, and Fluid Inclusion Characteristics of the Tuvatu Gold-Silver Telluride Deposit, Fiji: Comparisons with the Emperor Deposit. Economic Geology 101 (1), 135–158. https://doi.org/10.2113/gsecongeo.101.1.135.

Schulz, B., Sandmann, D., Gilbricht, S., 2020. SEM-based automated mineralogy and its application in geo-and material sciences. Minerals 10 (11), 1004.

Shock, E. L. (2007). *An updated and augmented version (slop07.dat) of the original SUPCRT92 database (sprons92.dat).*.

Sillitoe, R.H., 2002. Some metallogenic features of gold and copper deposits related to alkaline rocks and consequences for exploration. Mineralium Deposita 37 (1), 4–13. https://doi.org/10.1007/s00126-001-0227-6.

Smith, D.J., Naden, J., Jenkin, G.R.T., Keith, M., 2017. Hydrothermal alteration and fluid pH in alkaline-hosted epithermal systems. Ore Geology Reviews 89, 772–779. https://doi.org/10.1016/j.oregeorev.2017.06.028.

Spry, P.G., Scherbarth, N.L., 2006. The gold–vanadium–tellurium association at the Tuvatu gold–silver prospect, Fiji: conditions of ore deposition. Mineralogy and Petrology 87 (3), 171–186. https://doi.org/10.1007/s00710-006-0128-6.

Tarkian, M., Hünken, U., Tokmakchieva, M., Bogdanov, K., 2003. Precious-metal distribution and fluid-inclusion petrography of the Elatsite porphyry copper deposit. Bulgaria. *Mineralium Deposita* 38 (3), 261–281. https://doi.org/10.1007/s00126-002-0336-x.

Taylor, G.K., Gascoyne, J., Colley, H., 2000. Rapid rotationof Fiji: Paleomagnetic evidence and tectonic implications. Journal of Geophysical Research 105 (B3), 5771–5781.

Wallier, S., Rey, R., Kouzmanov, K., Pettke, T., Heinrich, C.A., Leary, S., O'connor, G., Tamas, C.G., Vennemann, T., Ullrich, T., 2006. Magmatic fluids in the Breccia-hosted epithermal Au-Ag deposit of Rosia Montana, Romania. Economic Geology 101 (5). https://doi.org/10.3929/ethz-b-000001689.

Werle, J.L., Ikramuddin, M., Mutschler, F.E., 1984. Allard stock, La Plata Mountains, Colorado—an alkaline rock-hosted porphyry copper – precious metal deposit. Canadian Journal of Earth Sciences 21 (6), 630–641. https://doi.org/10.1139/e84-069.

Wharton, M.R., Hathway, B., Colley, H., 1995. Volcanism associated with extension in an Oligocene-Miocene arc, southwestern Viti Levu, Fiji. Geological Society, London, Special Publications 81 (1), 95. https://doi.org/10.1144/GSL.SP.1994.081.01.06.

Wood, S.A., Mountain, B.W., Pan, P., 1992. THE AOUEOUS GEOCHEMISTRY OF PLATINUM, PALLADIUM AND GOLD: RECENT EXPERIMENTAL CONSTRAINTS AND A RE.EVALUATION OF THEORETICAL PREDICTION. Canadian Mineralogist 30 (4), 955–982.